Gondwana Research 23 (2013) 574–594

Contents lists available at SciVerse ScienceDirect

Gondwana Research

journal homepage: www.elsevier.com/locate/gr

GR Focus Review

Chemical sedimentary protoliths in the >3.75 Ga Nuvvuagittuq Supracrustal Belt (Québec, Canada)

A.M. Mloszewska [a,*], S.J. Mojzsis [b,c], E. Pecoits [a], D. Papineau [d,e], N. Dauphas [f], K.O. Konhauser [a]

[a] Department of Earth and Atmospheric Sciences, 1-26 Earth Sciences Building, University of Alberta, Edmonton, Alberta, Canada T6G 2E3
[b] Department of Geological Sciences, University of Colorado at Boulder, 2200 Colorado Avenue UCB 399, Boulder, CO 90309-0399, USA
[c] Laboratoire de Géologie de Lyon, Université Claude Bernard Lyon 1 and École Normale Supérieure de Lyon, CNRS UMR 5276, 2 rue Raphaël DuBois, Bât. Géode 3e, Villeurbanne, France
[d] Department of Earth and Environmental Sciences, Boston College, Chestnut Hill, MA 02467, USA
[e] Geophysical Laboratory, Carnegie Institution of Washington, Washington, DC 20015, USA
[f] Origins Laboratory, Department of Geophysical Science and Enrico Fermi Institute, The University of Chicago, 5734 South Ellis Avenue, Chicago, IL 60637, USA

ARTICLE INFO

Article history:
Received 18 May 2012
Received in revised form 7 November 2012
Accepted 13 November 2012
Available online 27 November 2012

Handling Editor: M. Santosh

Keywords:
Nuvvuagittuq
Archean
Banded iron formation
Seawater
Metallo-enzymes
Geochemistry

ABSTRACT

Analyses of chemical sedimentary precipitates such as banded iron formation (BIF) provide a direct means to explore the nature and composition of the early hydrosphere. The recently discovered >3750 Myr old Nuvvuagittuq Supracrustal Belt (NSB) in the Northeast Superior Province (Québec, Canada) hosts a suite of iron oxide-rich (±pyroxene and amphibole) units that are interpreted to be the metamorphosed equivalents of Fe oxide-facies BIF, and a collection of BIF-like Ca–Fe–Mg silicate rocks. The NSB rocks provide a rare glimpse of trace metal availability in Eoarchean (ca. 3800 Ma) seawater. As they may be contemporaneous with the relatively well-studied Isua Supracrustal Belt of southern West Greenland, their comparison provides an opportunity to enhance our basic understanding of the Eoarchean oceans at a global scale. Work since the initial discovery of the NSB in 2001 has established the basic lithological, geochemical and petrographic characteristics of these BIF and BIF-like rocks. Here we review the current state of knowledge of NSB rocks of probable chemical sedimentary origin, including aspects of their geology, likely origin and age. We conclude by examining the implications of results thus far for our understanding of early seawater compositions, and for the emergence of life in the context of early metallo-enzyme evolution.

Contents

* Corresponding author. Fax: +1 780 492 2030.
E-mail address: mloszews@ualberta.ca (A.M. Mloszewska).

1342-937X/$ – see front matter
http://dx.doi.org/10.1016/j.gr.2012.11.005

1. Introduction

Geological evidence for the earliest evolution of the Earth's surface system comes from a mere handful of localities older than about 3600 Ma. These include the Itsaq Gneiss Complex of West Greenland (ca. 3650–3850 Ma; Nutman et al., 1996); Nulliak Supracrustal Association of northern Labrador (≥3776 Ma, Schiotte et al., 1989); Narryer Gneiss Complex of western Australia (≤3730 Ma, Kinny et al., 1988); the Anshan area and Caozhuang Complex of northern China (≥3800 Ma, Jahn et al., 1987; Liu et al., 1992); Napier Gneiss Complex of Antarctica (≤3930 Ma, Black et al., 1986), Acasta Gneiss Complex of the Northwest Territories in Canada (3960–4060 Ma, Bowring and Williams, 1999), and the Nuvvuagittuq Supracrustal Belt of the Inuksuaq Complex in northern Québec (ca. 3800 Ma, Simard et al., 2003). Table 1 presents a summary characterizing these locations. Although many of these Hadean–Eoarchean terranes (nomenclature of Bleeker, 2004) are documented to contain supracrustal enclaves of probable volcanic and volcaniclastic derivation in the form of an assortment of mafic and ultramafic amphibolites, other variably deformed quartz (SiO_2) + magnetite (Fe_3O_4) ± amphibole ± pyroxene rocks are also found within them. The gross mineralogical and compositional characteristics of these rocks point to an origin as BIF and related sediments in that they are iron-rich (20–40 wt.% Fe_2O_3) and siliceous (40–60 wt.% SiO_2), typically with low Al_2O_3 (<1 wt.%) and low concentrations of relatively insoluble elements (Ti, Zr, Th, Hf and Sc<20 ppm). The latter two geochemical features are indicative of minimal detrital input during deposition. Although low detrital input is a general feature of these kinds of rocks, it does not hold true for all iron-formations (Klein, 2005).

Provided that the compositional spectrum of metamorphosed ferruginous–siliceous rocks encountered in Eoarchean terranes can be shown to have BIF as their protoliths, and given that such rocks precipitated directly from seawater (Trendall, 2009), their composition may preserve clues about the chemistry of Earth's earliest oceans. A number of studies have attempted to derive ancient marine compositions via the application of experimentally-derived partition coefficients to absolute whole-rock trace element abundances recorded in BIF (Konhauser et al., 2009 for nickel; and Mloszewska et al., 2012 for nickel and zinc; Planavsky et al., 2010b for phosphorus). Yet, for these systems to be used as effective seawater proxies for minor and trace elements, the effects of post-depositional remobilization on BIF compositions must be shown to have been minimal. This prerequisite is not easy to establish. All Eoarchean rocks thus far described are preserved as deformed supracrustal enclaves within granite–granitoid gneiss complexes that have had a protracted metamorphic history to at least amphibolite facies (>500 °C, >5 kbar; Nutman et al., 2004). Comparative rare earth element and yttrium (REE + Y) profiles are commonly used to probe the degree of alteration and remobilization of trace metals in BIF, as these are relatively immobile up to amphibolite metamorphic facies. In many cases, it has been fortuitous that BIFs show coherent seawater-like behavior, which suggests that these chemical sediments potentially record the chemical conditions of seawater at the time of their deposition (e.g., REE + Y, Bolhar et al., 2004; Dauphas et al., 2007b; cf. Johannesson et al., 2006).

It also remains an intriguing possibility that BIFs preserve both direct and indirect evidence of the activity of an early microbial biosphere that made extensive use of metals dissolved in seawater. First, the iron oxide minerals that constitute BIF have been implicated as by-products of biological Fe(II) oxidation in the photic zone of the Archean ocean (Dauphas et al., 2004; Konhauser et al., 2007; Johnson et al., 2008). These biological processes can either include the direct oxidation of Fe(II) by a group of anoxygenic photosynthetic bacteria termed photoferrotrophs. These bacteria use Fe(II) as a reductant for the conversion of CO_2 into organic biomass (Konhauser et al., 2002; Kappler et al., 2005). Another possibility is that the predecessors to cyanobacteria generated oxygen as a by-product of their metabolism, and that oxygen then reacted abiotically with dissolved Fe(II) to form ferric oxyhydroxides (Cloud, 1973). Second, from the standpoint of metallomics, the strict trace metal requirements of many basic enzymes in modern-day microbes were likely established by trace metal availability in the environment of their ancestors (Nisbet and Fowler, 1996; Anbar and Knoll, 2002). In principle, the genomes of deeply branching microbial communities might retain an archive of trace metal availability in the ancient oceans (daSilva and Williams, 2001; Saito et al., 2003). Such indirect inferences about the co-evolution of the biosphere with changes in metal availability of the hydrosphere can be tested directly by studying the evolution of the minor and trace element compositions of BIF. Third, in the ca. 3770 Ma Isua Supracrustal Belt (ISB) and the ca. 3830 Ma Akilia Association of the Itsaq Gneiss Complex in West Greenland, BIFs with ^{13}C-depleted graphite associations in apatite grains have been proposed as remnants of the activity of ancient microorganisms (e.g., Mojzsis et al., 1996). Some graphite associated with apatite in the Akilia quartz–pyroxene rock was most likely crystallized during a granulite facies metamorphic event in the Eoarchean and preserves characteristics consistent with – but not proof of – biological carbon (Schidlowski et al., 1979; Schidlowski, 1988; Rosing, 1999; Papineau et al., 2010a, 2010b). It was pointed out by Lepland et al. (2011) that other graphite occurrences from these rocks were clearly fluid-deposited later in the history of the rock and the possibility of several sources of carbon for the Akilia graphite can therefore not be excluded. Metamorphic decarbonation of ferruginous carbonates has been invoked as an alternate, abiotic mechanism for graphite formation in the Isua rocks (Perry and Ahmad, 1977), including those associated with apatite (van Zuilen et al., 2002, 2003, 2005). Graphitic coatings intimately associated with apatite have also been found in the Nuvvuagittuq BIF from northern Québec, but the poorly crystalline structure of these carbonaceous particles as well as their petrographic relation with low-temperature alteration minerals indicates either fluid deposition and/or remobilization of the reduced carbon, as well as late crystallization after the peak metamorphic event (Papineau et al., 2011). Due to the long and complex metamorphic history of all Eoarchean BIFs thus far documented, disagreement persists over the origin of graphite with variably depleted ^{13}C carbon isotope compositions in the oldest rocks (e.g., McKeegan et al., 2007). The search for biosignatures is obviously

challenging, and thus, evidence of ancient life must be sought through a range of complementary approaches.

The discovery of the NSB offers a unique and complementary opportunity to enhance what we know about the earliest oceans, via its comparison with the compositions to those of the better-studied West Greenland localities. Results thus far show that the NSB hosts rocks of chemical sedimentary origin compositionally similar to those from the ISB, and like them, the Nuvvuagittuq BIFs retained their seawater-like REE + Y profiles and do not have a significant detrital component (Dymek and Klein, 1988; O'Neil et al., 2007; Mloszewska et al., 2012). Although research on the NSB is still in its infancy, several studies subsequent to the initial discovery have established the basic characteristics of rocks with sedimentary protoliths (e.g., David et al., 2002; Simard et al., 2003; Cates and Mojzsis, 2007; Dauphas et al., 2007a; O'Neil et al., 2007). Research has progressed enough to warrant an assessment of the current state of knowledge. Here we provide an overview of the geology, age and origin of chemical sedimentary rocks of the Nuvvuagittuq Supracrustal Belt, their implication for early seawater composition, and for the emergence of life, especially in the context of the early evolution of microbial metalloenzymes.

2. Geological framework

The Nuvvuagittuq Supracrustal Belt (NSB) is situated on the northern shore of Hudson Bay approximately 1500 km north of Montréal, and 30 km south of the town of Inukjuak. It is part of a collection of roughly a dozen large (kilometer-scale) supracrustal enclaves distributed over a large area. They are rafted and tectonically juxtaposed within deformed gneisses of the Northeast Superior Province (NESP), which itself is part of the larger Superior Craton in northern Québec, Canada. The protoliths of NESP gneisses are dominantly plutonic rocks of TTG (tonalite–trondhjemite–granodiorite) and GGM (granite–granodiorite–onzonite) compositions that surround and, in some cases, intrude pyroxene-rich supracrustal assemblages, as well as amphibolite-ultramafic assemblages with basalt–komatiite compositions, bimodal amphibolites of broad tholeiitic to alkaline-basalt affinity (many with unusual Ca-depletion manifest as cummingtonite-rich amphibolites), and calc-alkaline felsic bodies (Boily et al., 2009). The NESP was previously divided into six major litho-tectonic domains based on the integration of structural and aeromagnetic data; each domain shows large linear positive and negative aeromagnetic anomalies that vaguely define structural boundaries (Stevenson et al., 2006 and references therein). The domains have a broadly NNW structural trend, and earlier studies suggested that, like other sub-provinces in the Superior Craton, the northeast part represents a series of volcanic arcs and back arc terranes that accreted at ca. 2700 Ma in the formation of this part of the Superior Province (Percival et al., 1994; Percival and Skulski, 2000). Subsequent whole-rock U–Pb and Sm–Nd geochronology has since resulted in the further subdivision of the NESP into two isotopically and magmatically distinct terranes: the Hudson Bay Terrane to the southwest and the Arnaud River Terrane to the northeast (Boily et al., 2009). The NSB is part of the Hudson Bay Terrane, the granite–granitoid gneisses of which are thought to be the product of Paleo- to Mesoarchean recycled crust.

In the conventional εNd notation defined as the departure of $^{143}Nd/^{144}Nd$ from the Chondrite Uniform Reservoir (CHUR) evolution line, these granitoids display some of the most depleted εNd values within the NESP (e.g., Boily et al., 2009). Moreover, the most depleted of these εNd values are prevalent in proximity to the Nuvvuagittuq belt (εNd: −27.4 to −9.3, David et al., 2002; O'Neil et al., 2008), indicating that the gneisses that enclose Nuvvuagittuq are likewise the product of extensive ancient recycled crust (Stevenson et al., 2006).

The overall structure of the NSB (Fig. 1) is a NNE oriented isoclinal synform refolded into a more open south-plunging synform with preserved bedding that strikes parallel to the steeply-dipping main schistosity (O'Neil et al., 2007; see Table 1). The Nuvvuagittuq rocks have been metamorphosed to at least upper amphibolite facies (Cates and Mojzsis, 2009) with the possible exception of the southwest corner (greenschist facies, assigned by O'Neil et al., 2007). They are bounded by ca. 3.66 Ga tonalites of the Voizel Suite, which in turn are surrounded by the 2.75 Ga granite–granitoid gneisses of the Boizard Suite (e.g., Simard et al., 2003; O'Neil et al., 2007 and references therein).

The most voluminous lithotype in the NSB is a compositionally unusual amphibolite that is typically cummingtonite-rich [$(Mg,Fe)_7Si_8O_{22}(OH)_2$] + biotite [$K(Mg,Fe)_3AlSi_3O_{10}(OH)_2$] + quartz ± plagioclase ± garnet ± phlogopite ± anthophyllite ± cordierite (O'Neil et al., 2007). It was colloquially termed "faux amphibolite" in earlier publications due to its low CaO contents and the absence of hornblende [$Ca_2(Mg,Fe,Al)_5(Al,Si)_8O_{22}(OH)_2$] as is more common of most other amphibolites (O'Neil et al., 2008). Recently, O'Neil et al. (2011) proposed a new unit name, "Ujaraaluk". This cummingtonite-rich rock is heterogeneous and varies widely in composition from CaO-poor amphibolites to garnet-bearing biotite schists; some of this variability is reflected in changes in alumina content. It has a banded texture with alternating biotite-rich and cummingtonite-rich banding at the centimeter scale that is especially evident on weathered surfaces. The cummingtonite amphibolites can also be characterized locally by an assemblage of cordierite (locally altered to chlorite and pinite), anthophyllite and biotite that is probably dependent on metamorphic grade. This is exemplified in the garnet content of the amphibolite unit that varies from almost none in the west to up to 50% in the east, and typically shows up as meter-scale alternating garnet-rich and garnet-poor bands (O'Neil et al., 2011). Quartz ribboning is also seen following the general direction of schistosity. It has been proposed that the amphibolites represent a metamorphosed mafic pyroclastic deposit (Cates and Mojzsis, 2007; O'Neil et al., 2007), or sub-mature mafic sediments that were albitized by early hydrothermal alteration (Cates et al., in press). Tabular ultramafic bodies occur in the belt which range from 5 to 30 m in thickness (interpreted by O'Neil et al., 2007, 2008 as sills, but cf. Cates and Mojzsis, 2007). They consist of serpentine [$(Mg,Fe)_3Si_2O_5(OH)_4$] + talc [$Mg_3Si_4O_{10}(OH)_2$] ± tremolite [$Ca_2Mg_5Si_8O_{22}(OH)_2$] ± hornblende ± chromite [$FeCr_2O_4$], and locally contain 10–20 cm thick hornblende-dominated, amphibole-rich layers. At outcrop scale, "gabbroic chilled margins" were claimed (O'Neil et al., 2011), which if they can be verified, would be further suggestive of differentiated intrusions.

2.1. Lithology and field relationships

Several quartz-rich schists whose protoliths were chemical sediments have been identified in the NSB (Fig. 2), and they share the deformation history of the rest of the belt. A 5 to 30 meter wide, finely-banded BIF outcrops continuously on the western fold limb and discontinuously on the eastern limb of the Nuvvuagittuq structure; a thin banded unit of calc-silicate rocks (called the banded silicate formation, or BSF, by Mloszewska et al., 2012) is ~50 to 60 m removed from the BIF, and a massive "silica formation" has also been mapped on the eastern fold limb (O'Neil et al., 2011). The BIF consists of magnetite + grunerite [$Fe_7Si_8O_{22}(OH)_2$] or cummingtonite + quartz ± hematite [Fe_2O_3] ± augite [$(Ca,Na)(Mg,Fe,Al,Ti)(Si,Al)_2O_6$] ± apatite [$Ca_5(PO_4)_3(F,Cl,OH)$] ± pyrite [$FeS_2$], and ranges from alternating magnetite and grunerite bands with quartz scattered throughout, to finely alternating (laminated) magnetite and quartz bands with thin grunerite bands in between. In the latter, the heterogeneous distribution of magnetite and quartz bands suggests that it might be a primary texture that was less affected by silica mobility and recrystallization during metamorphism. Jaspilites are very locally associated with dark-green amphibolites in the south west corner of the belt, as well as with chert- and metacarbonate rocks (Fig. 2; David et al., 2009; Papineau, 2010; Cates et al., in press). Field relationships show that anastomosing mm- to cm-thick jaspilite, carbonate, and chert veinlets in the surrounding amphibolite coalesce in the metacarbonates and jaspilite BIF. It seems therefore that the jaspilite and metacarbonate rocks are part of a later,

post-deformational, hydrothermal circulation event subsequent to deposition of the cummingtonite-amphibolite unit.

Another feature of the BIF is that they seem to act as a compositional boundary between two chemically distinct groups of cummingtonite-amphibolite units (as defined primarily by their Al/Ti ratios and REE profiles; O'Neil et al., 2011). The high-Ti amphibolite unit occurs stratigraphically "inboard" of the BIF in the direction of the belt's fold axis; it ranges in composition from basaltic, to basaltic–andesitic and dacitic, and has low Al/Ti ratios and relatively flat REE profiles. In contrast, the low-Ti unit, which ranges more narrowly in composition from basaltic to basaltic–andesitic, can be further subdivided in two groups; the one immediately adjacent to the BIF has the highest Al/Ti ratios and U-shaped REE profiles, whereas the one inboard of the BIF toward the very center of the belt displays large negative Ta and Nb anomalies and enriched LREE profiles (O'Neil et al., 2011). It has been postulated that the geochemical transition defined by the BIF represents a real transition between rocks of more tholeiitic character to more calc-alkaline ones (O'Neil et al., 2011). Finally, calc-silicate rocks that consist of quartz + grunerite ± magnetite ± actinolite [$Ca_2(Mg,Fe)_5Si_8O_{22}(OH)_2$] ± augite ± pyrite occur as alternating bands of grunerite and quartz, with magnetite scattered throughout the grunerite bands. Actinolite is commonly present as thin exsolution lamellae within grunerite host grains in a texture associated with retrograde hydration metamorphism (Ross et al., 1969).

3. Geochronology

There are three main challenges to establishing absolute ages for ancient supracrustal belts: (i) the rocks are dominantly amphibolites which rarely contain primary igneous zircons that can be reliably dated via the U–Pb method; (ii) they are highly deformed so that primary contact relationships may be blurred or erased, thus complicating interpretations of relative emplacement times; and (iii) metamorphism and recrystallization can complicate radiogenic isotope systems (Rb–Sr, Sm–Nd, U–Pb). Accordingly, means of providing a maximum age constraint on the time of amphibolite emplacement and the rest of the supracrustal package must usually be established with less direct techniques. That all known Eoarchean rocks have been strongly overprinted by a complex geologic history requires a detailed approach of local high-resolution mapping that directs sample collection for geochronology at the appropriate scale of the outcrops (e.g., 1:250 or less).

3.1. Minimum age assignment for the NSB

The minimum age of ca. 3750 Ma for emplacement of the NSB was established from ID-TIMS and ion microprobe U–Pb zircon geochronology for felsic (trondhjemitic) gneiss sheets that cross-cut the amphibolites (David et al., 2002; Cates and Mojzsis, 2007; David et al., 2009). High-resolution (1:50 scale) mapping of key outcrops in the NSB (e.g., David et al., 2009) revealed that these gneisses occur as narrow sub-meter intrusions in amphibolites (previously termed "felsic bands") and in rare cases these transect primary lithotype boundaries (Cates and Mojzsis, 2007). Samples from the Porpoise Cove trondhjemitic gneisses of the NSB show that the oldest and least-disturbed (within 5% of concordia) zircon cores define a statistically robust $^{207}Pb/^{206}Pb$ vs. $^{238}U/^{206}Pb$ intercept age of 3758^{+51}_{-47} Ma (Cates and Mojzsis, 2007; Figs. 3, 4; Table 1).

Aspects of the timing and intensity of the protracted metamorphic history of the NSB were further elucidated from coupled Ti-in-zircon thermometry (Ti^{xln}), comparative analysis of $[Th/U]_{zrc}$, zircon/rock REE lattice-strain modeling, mineral-pair thermobarometry, and ion microprobe U–Th–Pb zircon depth profiling of these felsic gneisses (Cates and Mojzsis, 2009). The depth profiles of two NSB zircons with concordant igneous cores (3802 ± 12; 3743 ± 26 Ma) yield ages that reproduce all previously reported igneous and metamorphic ages for the Nuvvuagittuq rocks and surrounding units in the NESP. Consequently, there is little doubt that the NSB is at least Eoarchean in age and perhaps contemporaneous to the ISB in West Greenland. Yet, unlike the ISB and the few other Eoarchean terranes so far known to exist, the NSB also preserves relatively abundant quartz–biotite schists (including possible meta-conglomerates) and chromite-bearing quartzites of likely detrital origin (Cates and Mojzsis, 2007; Dauphas et al., 2007a; Cates et al., in press). These are now known to contain detrital zircons that provide a means toward constraining an upper boundary age of the Nuvvuagittuq Supracrustal Belt.

3.2. Maximum age assignment for the NSB

Candidate detrital zircons have been found in quartz–biotite schists sampled at Nuvvuagittuq (Cates and Mojzsis, 2007; David et al., 2009). These units were described as being several centimeter- to meter-scale with laterally continuous quartz–biotite layers dominated by strongly *S*-deformed (aspect ratio ~10:1) polymict quartz clasts in a matrix of biotite with disseminated quartz, and minor garnet. The mineralogy of these rocks is dominated by quartz and biotite, with minor pyrite, magnetite, zircon and clinozoisite (Dauphas et al., 2007a). Although the quartz–biotite rocks are a minor lithotype in the NSB, they are nevertheless part of the same supracrustal succession which includes the cummingtonite-amphibolite rocks and they share all of the deformation history of the belt. One of these quartz–biotite units, contiguous to hornblende-amphibolites and within 50 cm of a 3758^{+51}_{-47} Ma trondhjemitic gneiss (Cates and Mojzsis, 2007), yielded a zircon population with an upper intercept U–Pb isochron age of 3787 ± 25 Ma (Cates et al., in press). These probable detrital zircon ages may be used to argue that emplacement of the supracrustals was coeval with the oldest granitoids. Indeed, exactly such a relationship was documented in zircon age populations from rare quartz–biotite schists captured in the similarly ancient gneiss terranes of southern West Greenland (Nutman et al., 2004).

Chromite-bearing quartzites containing Cr-rich muscovite occur in the NSB as thin (cm-scale), laterally continuous (10s m-scale) green to greenish-gray rock exposures that share knife-edge contacts with the surrounding units, including the cummingtonite-amphibolites, hornblende-amphibolites and quartz–biotite schists. Mineralogically, the quartzites are dominated by quartz (70–80%), with about 10% plagioclase, and the remainder comprises phylosillicates (including Cr-rich muscovite), oxides, sulfides, and zircons. They are poor in Ca and the alkali metals ($CaO + Na_2O + K_2O < 3$ wt.%) and have high Ni (>50 ppm) and Cr (>140 ppm) contents belying their origin as placer deposits (Cates et al., in press). Rare earth and multi-element plots for the quartzites are similar to previously published patterns for the quartz–biotite schists. Whole-rock analyses of the quartzites show sub-chondritic Y/Ho ratios (<31), and similar to the quartz–biotite units (26–28), oxygen has heavy $\delta^{18}O$ values (+10‰; Cates et al., in press). Importantly, they yield abundant zircons and have distinct age populations. The oldest $^{207}Pb/^{206}Pb$ age population (3730 to 3780 Ma; n = 13) clusters around 3742 Ma and comprises rounded (mechanically abraded) and oscillatory-zoned zircon cores that display thin overgrowths as seen in back-scattered electron imagery (Cates et al. in press). Rarely, these zircons show weak internal oscillatory zoning when compared to the younger (metamorphic) populations, which are dominated by sector, irregular or mundane zonations; the youngest population is typified by "spongy" internal structures akin to that described for hydrothermal growth (Hoskin and Schaltegger, 2003; Cates et al., in press). Zircon $[Th/U]_{zrc}$ of the different age populations are in accordance either with equilibrium growth in a granitic melt (oldest grains) or various modes of metamorphic growth (Cates and Mojzsis, 2009; Cates et al., in press). Comparisons of detrital and igneous zircon ages from multiple detrital lithologies in the NSB show that its initial development probably took place around 3800 Ma and

Table 1
Table summarizing the main characteristics of the major Eoarchean-aged rock occurrences world-wide.

Location	Structure	Major lithologies	Metamorphic grade	Age	References
Nuvvuagittuq Supracrustal Belt (N. Quebec, Canada)	Tight NNE-oriented isoclinical synform, refolded into more open, S-plunging synform	Cummingtonite-rich amphibolites; trondjhemite gneiss; gabbroic and peridotitic conformable bodies; chemical sedimentary rocks	Upper-amphibolite facies; major metamorphic events at 2.7 Ga, and 3.6 Ga	Min. age of 3750 (U–Pb zircon age); max. age of 4280 Ma (^{146}Sm–^{142}Nd isochron age)	e.g., Simard et al. (2003), Cates and Mojzsis (2009) and O'Neil et al. (2007, 2008)
Itsaq Gneiss Complex (SW. Greenland)	NE–SW trending belt, bounded by the Akia Terrane to the NW, and by the Tasiusarsuaq Terrance to the SE	The 3.57–3.87 Ga quartzofeldspathic Amitsoq Gneisses; the 3.7–3.8 Ga Isua Supracrustal Belt; the 3.2–3.5 Ga basic Ameralik Dykes	Amphibolite to granulite facies; major metamorphic events at ca. 3.6 and 2.7 Ga	Max. ^{207}Pb/^{206}Pb zircon age of 3850 Ma, and min. age of 3560 Ma	e.g., Nutman et al. (1996, 2000) and Nutman et al. (1997)
Nulliak Supracrustal Association (N. Labrador, Canada)	Disseminated outcrops within the 3.7 Ga Uivak Gneisses	Gabbroic, clinopyroxinitic & peridotitic amphibolites; quartzofeldspathic & garnet–sillimanite gneisses; chemical sedimentary rocks	Upper amphibolite to granulite facies; major metamorphic events at 2.9 Ga and 3.6 Ga	Max. age of 3776 Ma (U–Pb zircon age)	e.g., Schiotte et al. (1989), Nutman et al. (1989) and Bridgewater and Schiötte (1991)
Narryer Gneiss Complex (W. Australia)	NE-trending 30,000 km^2 belt on the western margin of the Yilgarn Craton	3.68 Ga Meeberie Gneiss; 3.4 Ga Dugel Gneiss; 3.73 Ga Manfred Complex (incl. BIF); 3.3 Ga metasedimentary rocks; 1.6–2.0 Ga basic dykes	Granulite-facies metamorphism ca. 3.3 Ga; subsequent retrogression to lower greenschist- and amphibolite-facies	Max. age of 3730 Ma; ca. Ga zircons found in the Jack Hills area	e.g., Kinny et al. (1988), Myers and Williams (1985) and Wilde et al. (2001)
Anshan area (N. China)	~2400 km^2 belt in the Eastern Block of the North China Craton	Trondhjemitic Baijifen Complex; granites and supracrustals (incl. BIF) of the Chentaigou Complex; granitic-supracrustal Teijiashan-Lishan Dome; Anshan-Qidashan Supracrustal Belt; Qidashan granite	Amphibolite facies, retrogressed in places to greenschist facies; major metamorphic events ca. 3.3 Ga, 2.5 Ga	Max. ^{207}Pb/^{206}Pb age of 3812 Ma (Baijifen Complex); min. age of 2475 Ma	e.g., Kaiyi et al. (1990), Zhai and Windley (1990), Liu et al. (1992) and Liu et al. (2007)
Caozhuang Complex (N. China)	Supracrustal rocks occur as discrete bodies within 3.5–2.5 Ga orthogneisses; Eastern Hebei Province, North China Craton	Caozhuang supracrustals (amphibolites; felsic gneisses; marbles; quartzites; calc-silicates and BIF); multiphase granite gneisses	Amphibolite to granulite facies	3860 Ma U–Pb SHRIMP age (zircon in quartzite)	e.g., Jahn et al. (1987), Kaiyi et al. (1990) and Liu et al. (2007)
Napier Gneiss Complex (Antarctica)	80,000 km^2 area in the East Antarctic Shield	Pyroxene–quartz–feldspar and garnet–quartz–feldspar gneiss; granite–pyroxenite rocks; siliceous, aluminous and ferruginous rocks; intrusive granites and mafic dykes	High granulite-facies; major metamorphic events at ca. 3.0 Ga, 2.9 Ga, and 2.5 Ga.	Max. U–Pb SHRIMP age of 3930 Ma	Black et al. (1986) and Harley and Black (1997)
Acasta Gneiss Complex (N. Canada)	Exposed in the Scotstoun and Exmouth Antiforms (forms the core of the latter) of the Wompay Orogen, on the Western margin of the Slave Craton	Quartz-dioritic and gabbroic gneisses; TTG and granite gneisses; mafic, intermediate and felsic gneisses; foliated granite	Amphibolite-facies metamorphism; major metamorphic events at ca. 3.6 and 3.5 Ga	Max. U–Pb SHRIMP zircon age of ca. 4030 Ma; min. age of 3960 Ma	e.g., Bowring and Williams (1999) and Iizuka et al. (2007) and references therein

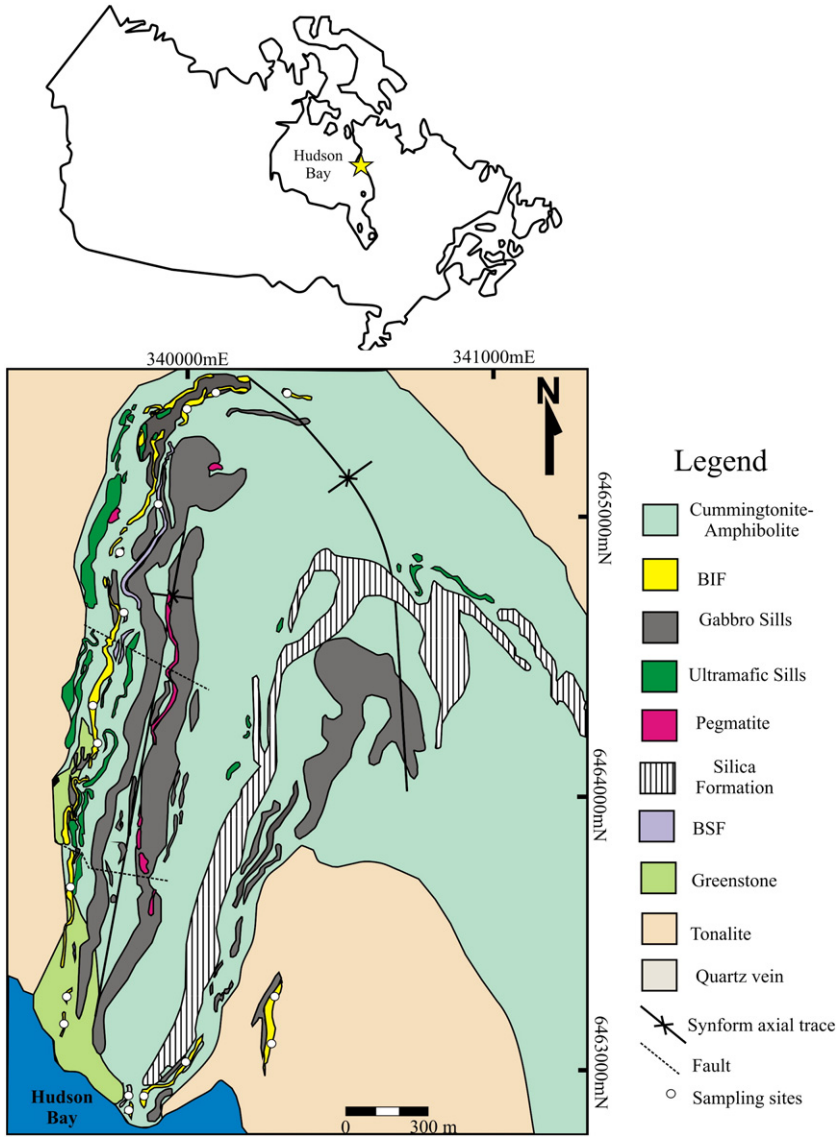

Fig. 1. Location map of the Nuvvuagittuq Supracrustal Belt (NSB). The belt is located in the Northeastern Superior Craton (NESP, northern Québec) on the northern shore of Hudson Bay. After David et al. (2009) and O'Neil et al. (2011).

perhaps over a time span of less than ~20 Myr, akin to the timescales of contemporary oceanic arc settings.

3.2.1. A proposed Hadean (ca. 4300 Ma) formation age for the NSB

The work of O'Neil et al. (2008) showed that the NSB cummingtonite-amphibolites record deficits in the daughter product (^{142}Nd) of the extinct radionuclide ^{146}Sm (t1/2 = 103 Ma; newly revised to 68 Ma, Kinoshita et al., 2012) which is expressed in the standard μ-notation as negative values vs. Bulk Silicate Earth (BSE). This was the first time that ^{142}Nd/^{144}Nd was measured to be lower than BSE. The reported degrees of depletion require that an enriched (low Sm/Nd) perhaps crustal source of these rocks was isolated from the ^{142}Nd isotopic evolution of BSE in the first few hundred million years while ^{146}Sm was still in the process of decaying to ^{142}Nd. In their study, O'Neil et al. (2008) tested the notion that negative μ^{142}Nd anomalies might reflect more than just the antiquity of an ancient felsic source, but could indicate the actual time of formation of the Nuvvuagittuq cummingtonite-amphibolites when they became separated from BSE. To this end they performed regressions through ^{142}Nd/^{144}Nd vs. ^{147}Sm/^{144}Nd space to construct a 4280^{+53}_{-81} isochron (revised to 4362^{+35}_{-54} with the new decay constant). This result is important because it shows that certain low Sm/Nd components that went into the formation of the Nuvvuagittuq belt survived from the earliest times of Earth's history.

Whether the age assignment of O'Neil et al. (2011) represents a time of formation of the NSB, or an inherited ^{142}Nd/^{144}Nd signal from a recycled source (Cates and Mojzsis, 2009; Cates et al. in press; Roth et al., (in press) and Guitreau et al., 2012) is currently the subject of debate. For instance, conventional ^{147}Sm–^{143}Nd isochron ages for the same rocks provide a statistically imprecise age of 3876 ± 191 Ma that is in general agreement with the U–Pb zircon ages. O'Neil et al. (2008) proposed that the ^{147}Sm–^{143}Nd ages, which are 500 Ma younger than the ^{142}Nd/^{144}Nd vs. ^{147}Sm/^{144}Nd regressions, arose from partial re-equilibration of the Sm–Nd system via one or more metamorphic events. In support of this idea, a 4023 ± 110 Ma ^{147}Sm–^{143}Nd isochron age was obtained for a younger, intrusive ultramafic body. However, it has also been argued that Nd depleted mantle model ages (T_{DM}) that are mostly younger than the ^{142}Nd/^{144}Nd vs. ^{147}Sm–^{143}Nd isochron ages for the same rock, are evidence of extensive Sm/Nd disturbance in this system (David et al., 2009). Combined ^{147,146}Sm–^{143,142}Nd geochronology from such disturbed systems is therefore problematic, including those that host negative ε^{142}Nd values. It is worth noting that similarly-aged rocks in West Greenland and western Australia also show deviations in ^{142}Nd/^{144}Nd

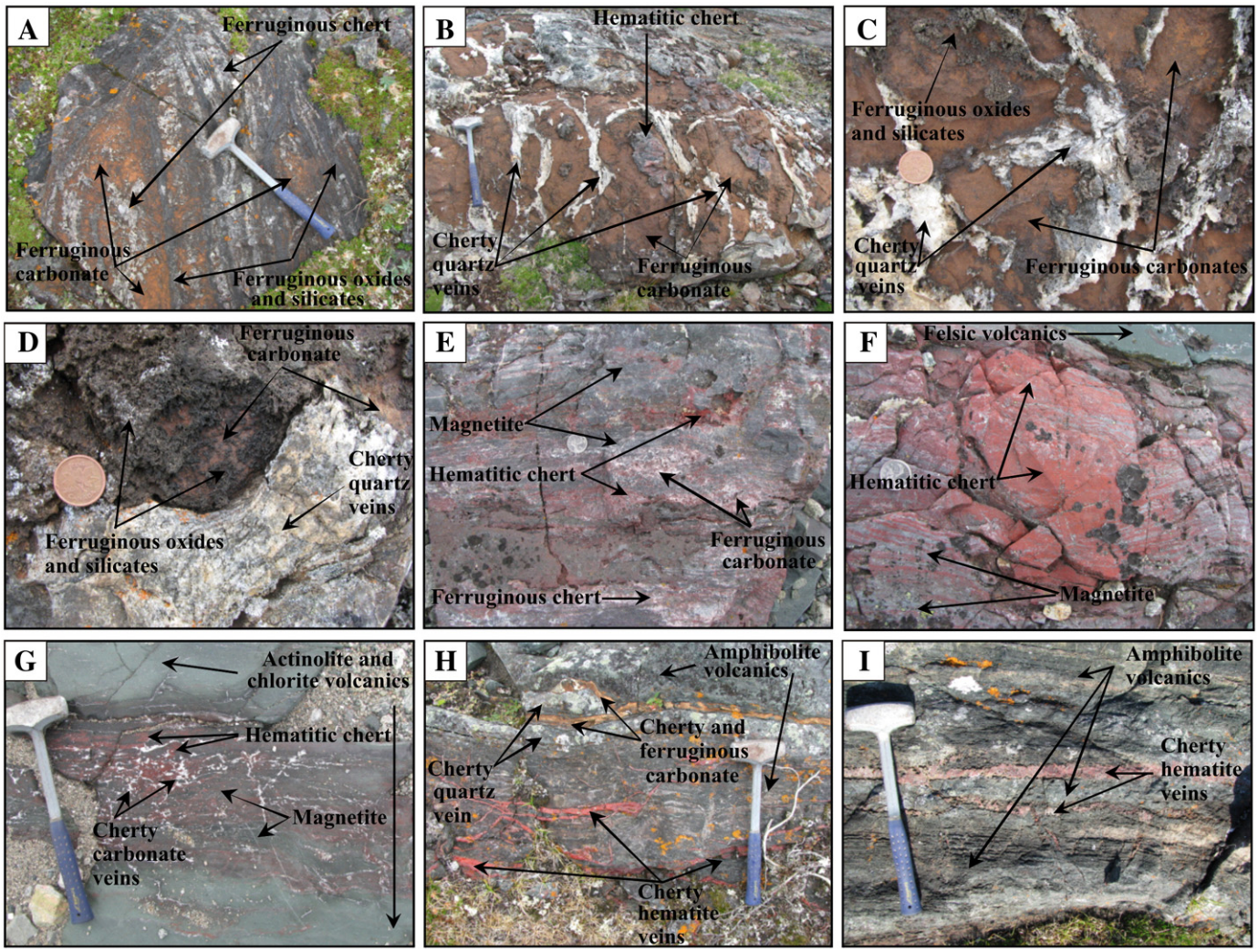

Fig. 2. Field images of outcrops on the eastern limb of the NSB. (A–C) Metacarbonate rocks dominated by quartz + magnetite + calcite + stilpnomelane ± ferruginous carbonate, (D–F) jaspilites with quartz + magnetite + hematite ± carbonate ± ferruginous silicates, and (H–I) cummingtonite-amphibolites with infiltrating veinlets of hematitic chert, ferruginous carbonate and cherty quartz.

vs. BSE. In these other Eoarchean examples, higher $^{142}Nd/^{144}Nd$ values (expressed in the conventional mu notation as positive $\mu^{142}Nd$) are contained in some amphibolites and garnet-bearing quartz–plagioclase biotite paragneisses from Isua (Boyet et al., 2003; Caro et al., 2006) and Akilia (Bennett et al., 2007). The age constraints provided by U–Pb zircon geochronology for the cross-cutting granitoid gneisses compared with those of the West Greenland Eoarchean supracrustals suggest that these rocks must have tapped an ancient (pre-4300 Ma) and depleted (high Sm/Nd) mantle reservoir when they formed at ca. 3770 Ma (Hamilton et al., 1983; Moorbath et al., 1977). It is also plausible that the slight positive correlations in $^{142}Nd/^{144}Nd$ vs. $^{147}Sm–^{143}Nd$ preserved in some parts of the Nuvvuagittuq belt may also reflect variable mixing of an older low $^{142}Nd/^{144}Nd$ end-member component with BSE at time of formation. Illustrative of this kind of inheritance is the report that lower $^{142}Nd/^{144}Nd$ ratios were also found (O'Neil et al., 2008) in samples of the ca. 3600 Ma Voizel suite granitic gneisses that envelope the NSB (David et al., 2009).

3.2.2. An Eoarchean formation age for the NSB

Detrital zircon ages of igneous derivation in quartzites of the Nuvvuagittuq Supracrustal Belt suggest that these rocks – including the cummingtonite-amphibolites that preserve low $^{142}Nd/^{144}Nd$ – may not represent relict Hadean mafic crust that formed ca. 4300 Ma but was instead captured in a supracrustal belt that may be no older than ca. 3780 Ma. Inheritance from pre-existing ancient Hadean crust explains the presence of $\mu^{142}Nd$ anomalies in all post-Hadean rocks thus far discovered (e.g., Boyet and Carlson, 2006). The absence of concordant pre-3800 Ma zircons in any NSB lithotype thus far analyzed implies that if the cummingtonite-amphibolites are of sedimentary rather than igneous origin, they were derived in part from reworked juvenile and non-zircon-bearing (albeit enriched low Sm/Nd) crustal components. As such, the various conventional Sm–Nd model ages of 4100–4400 Ma (O'Neil et al., 2007; David et al., 2009) represent their average sedimentary provenance age (e.g., Yamashita et al., 2000). Otherwise, if NSB cummingtonite amphibolite protolith was volcanic, negative $\mu^{142}Nd$ values became assimilated from remelting of older mafic crust.

4. Petrography and paragenetic interpretation of the NSB chemical sedimentary rocks

On the basis of mineral assemblages, Mloszewska et al. (2012) recognized two broad types of sedimentary lithologies in the Nuvvuagittuq Supracrustal Belt, banded iron formation (BIF) and banded silica formation (BSF). The mineralogy of the BIF consists of alternating layers of magnetite, grunerite ± augite and quartz, whereas the BSF contains

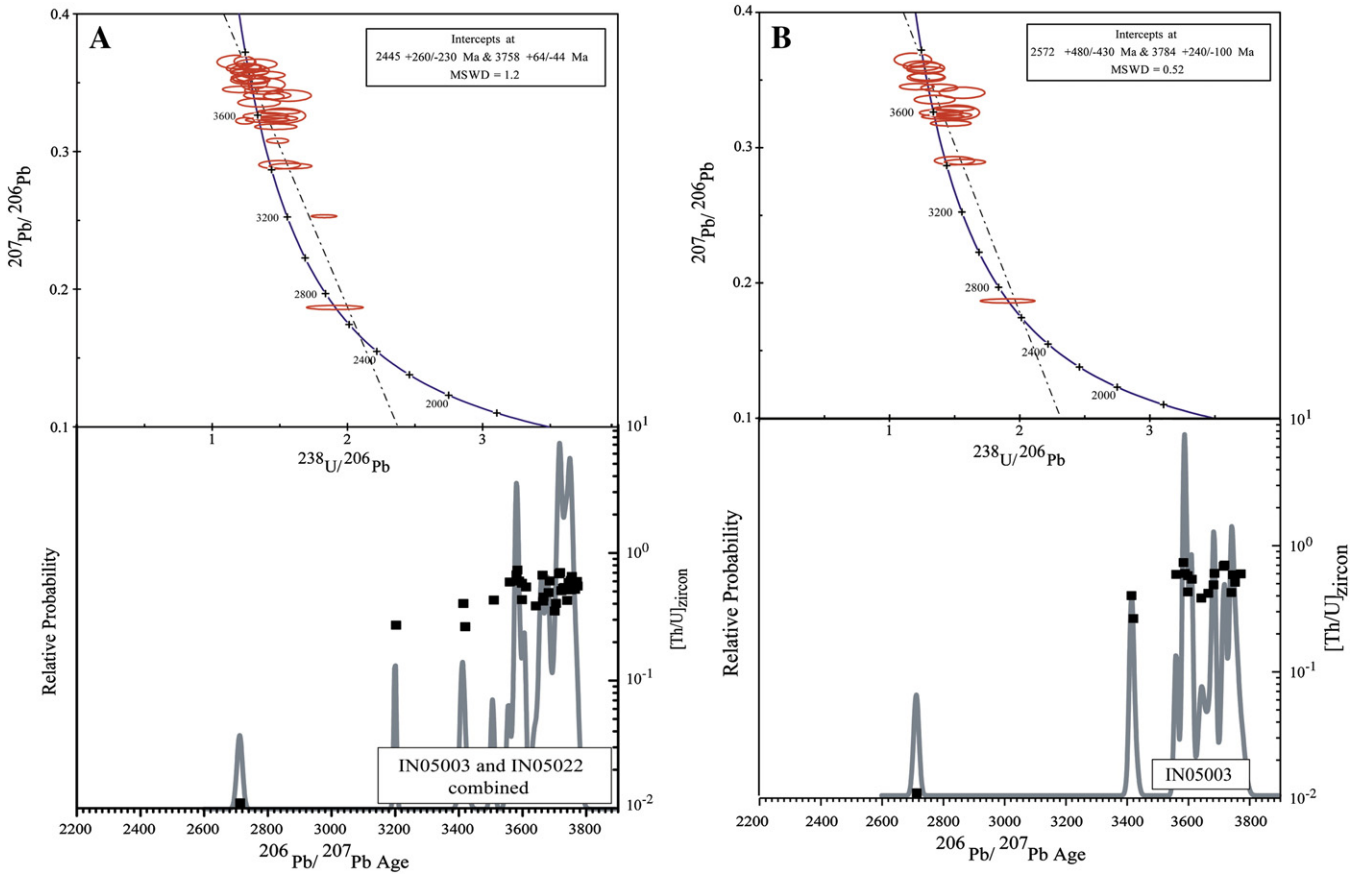

Fig. 3. Integrated geochronology and Th/U geochemistry from trondhjemitic gneisses in the NSB. The upper panels are Terra–Wasseberg plots where each population corresponds to separate events (1σ error ellipses). The lower panels show integrated probability and $[Th/U]_{zircon}$, where the gray fields are $[Th/U]_{zircon}$ predicted from whole-rock geochemistry. After Cates and Mojzsis (2009).

augite, grunerite, actinolite and quartz as the main mineral phases. In both rock types, the fine sub- to centimeter-scale lamination is largely defined by the relative abundance of their components, which define 'iron-rich' and 'iron-poor' layers. Magnetite occurs as a dominant constituent of the BIF (20–40 modal%) and as a minor constituent of the BSF (0.5–10 modal%). In the latter, the 'iron-rich' bands consist of Fe- and Ca-bearing amphiboles and pyroxene (≤50 modal%). Locally these bands are up to 5 cm thick and the presence of amphiboles and pyroxene imparts a dark green color to these layers. BIFs show a finer and more regular banding and a light- to dark-brown color due to the abundance of magnetite and grunerite ± augite microlayers. As previously mentioned a third sub-type of chemical sediment, a jaspilite, has recently been recognized in the NSB. The jaspilites described here occur in a localized area in the south-west corner of the belt, and they have also been observed in a localized outcrop in the north-east part of the belt (O'Neil, personal communication). See Table 2 for a summary of the mineralogy and petrography of each of these rock types.

4.1. BIF petrography

Iron-rich laminae in the BIF are largely composed of magnetite with minor or absent grunerite and augite. Typical BIF mineral assemblages and textures are illustrated in Fig. 5A–D. Magnetite-rich microlaminae consist of massive aggregates and subhedral crystals (0.04–0.2 mm). Small subhedral crystals also occur dispersed in 'iron-poor' laminae and as inclusions in all the other minerals. Quartz layers occur interbedded with magnetite layers and are found in conjunction with grunerite and augite, although pure quartz layers are also observed. The ratio of grunerite/quartz is highly variable depending on sample location. Quartz makes up to 50 modal% and as low as 20%, while grunerite ranges from 10 to 40%. Quartz forms anhedral grains, up to 1 mm across, and displays straight and marked undulose extinction. The grunerite shows anhedral to subhedral laths, up to 1 cm in length. The grunerite can be found associated with both the magnetite-rich laminae and the quartz-rich laminae, but it also forms massive layers between them. Grunerite has inclusions of magnetite, quartz and smaller grunerite crystals. Augite is also associated with both grunerite and magnetite bands. It occurs as individual anhedral to subhedral grains up to 0.2 mm in size, commonly with inclusions of quartz and magnetite, and can also be found as an inclusion in grunerite. Scarce calcite patches, up to 0.5 cm long, have been identified in the south of the western limb of the NSB. Inclusions of corroded quartz and magnetite indicate that calcite is a late-stage mineral phase.

4.2. BSF petrography

The BSF mainly consists of augite, actinolite, grunerite and quartz, together with minor biotite, magnetite, pyrite, chlorite and calcite. When microbanding is present, the preferred orientation of elongated prismatic amphiboles and pyroxenes in the green layers and granular quartz in the white layers gives the rock a grano-nematoblastic texture (Fig. 5E–F). Quartz makes up to 60 modal% of the BSF. Crystals normally display undulose extinction and occasionally the presence of elongated subgrains and sutured boundaries. Quartz varies from 0.5 to 6 mm in size and contains inclusions of actinolite, augite and

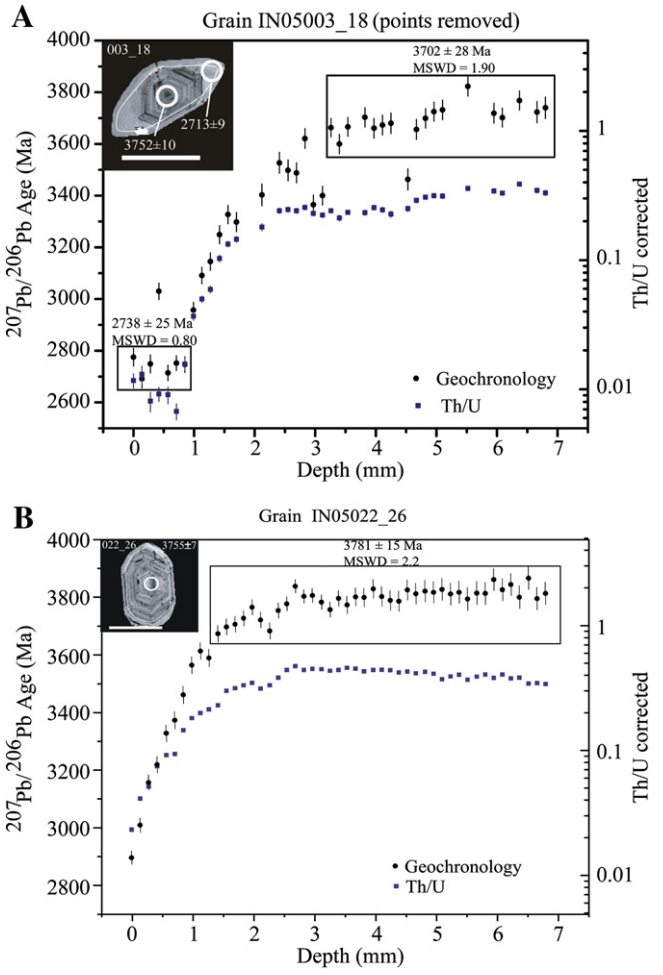

Fig. 4. U–Pb vs. depth profiles for zircons (IN05022_26, and IN05003_18) from a trondhjemitic gneiss, and corresponding Th/U ratios. Boxed areas represent the analyses used to determine the latter. Inset: Backscatter electron images of these zircons; ages (in Ma) were determined by standard ion probe techniques.
After Cates and Mojzsis (2007, 2009).

magnetite. Euhedral to subhedral augite crystals, commonly between 0.5 and 1.5 mm long, occur in bands associated with actinolite. The latter is pleochroic, ranging from dark green to pale yellow, which is likely due to high Fe content. They show two distinct habits of euhedral to subhedral laths, 1 to 3 mm long, and small (0.1–0.5 mm) irregular grains. The actinolite contains inclusions of magnetite, quartz and augite. Exsolution lamellae of Ca-amphibole in grunerite, oriented parallel to the (001) lattice planes, are common locally. Biotite is pleochroic from dark brown to straw-yellow and forms scattered subhedral to euhedral flakes, up to 2 mm in length, and much smaller grains as inclusions in the actinolite. Although it is an accessory mineral, biotite can be important locally. Pyrite and magnetite form subhedral scattered grains, up to 2 mm across and rarely exceed 2% of the rock. Calcite and chlorite are unusual in the BSF and occur as interstitial phases. The green pleochroic chlorite is a ferroan variety of clinochlore (ripidolite, $(Mg,Fe)_9Al_6Si_5O_{20}(OH)_{16}$) and displays abnormal violet or blue interference colors.

4.3. Jaspilite petrography

These rocks are composed of quartz, calcite, magnetite, hematite, and contain some ferruginous silicates, such as stilpnomelane [$K(Fe,Mg)_8(Si,Al)_{12}(O,OH)_{27}$] (Fig. 6). Anhedral quartz grains vary between 1 mm and sub-micron in size and the larger grains are often rimmed by veined magnetite. Magnetite also occurs as discontinuous bands of anhedral to euhedral grains, and these bands are commonly cross-cut by quartz–hematite veinlets or truncated by small normal faults. Hematite tends to occur dominantly along coarse quartz grain boundaries, but it also occurs as finely disseminated micron-size flakes in fine-grained quartz and calcite. This is especially common when calcite forms rounded structures in fine-grained quartz (Fig. 6C–E), but these rounded structures also occur as thin hematite ribbons in quartz. Finely disseminated hematite in quartz commonly forms thin ribbons that vary in shape between rounded or sub-spherical structures to stretched and elongated structures (Fig. 6F–G). Acicular grains of stilpnomelane also occur, and are often mixed with quartz, calcite, and magnetite. Other accessory minerals include anhedral fluorapatite crystals between 0.002 and 0.015 mm in size as well as mm-size anhedral chalcopyrite crystals.

4.4. Mineral paragenesis

The BIF and BSF tend to show highly recrystallized textures, which makes it very difficult to distinguish relict minerals or primary textures. Magnetite and quartz occur in most metamorphic BIF assemblages, resulting from the recrystallization of Fe-oxide and silica precursors, respectively. One of the most conspicuous minerals in the medium-grade metamorphosed BIF is cummingtonite–grunerite, which can be formed as a result of reaction between Fe-rich carbonates such as ferrodolomite [$Ca(Fe,Mg)(CO_3)_2$], and quartz, and as a reaction product of minnesotaite [$7Fe_3Si_4O_{10}(OH)_2$] (Klein, 2005), as follows [reaction 1]:

$$7Ca(Fe,Mg)(CO_3)_2 + 8SiO_2 + H_2O \rightarrow (Fe,Mg)_7Si_8O_{22}(OH)_2 + 7CaCO_3 + 7CO_2 \quad (1)$$

$$7Fe_3Si_4O_{10}(OH)_2 \rightarrow 3Fe_7Si_8O_{22}(OH)_2 + 4SiO_2 + 4H_2O. \quad (2)$$

Either of these reactions could have produced the cummingtonite–grunerite that occurs in the Nuvvuagittuq banded formations, but iron isotopes support derivation of at least some of the cummingtonite–

Table 2
Table summarizing the mineralogy, modal % and general petrography of the Nuvvuagittuq BIF, BSF and jaspilite.

Rock type	Magnetite	Hematite	Grunerite	Actinolite	Augite	Quartz	Stilpnomelane	Carbonate	Accessory minerals	Petrography
BIF	x 20–40%		x 10–40%		x <5%	x 10–60%			x <2%	Alternating, regularly-banded sub-to cm-scale iron rich (magnetite ± quartz grunerite ± augite) and iron poor (quartz + grunerite ± augite) laminae
BSF	x 0.5–20%		x <50%	x	x	x <60%			x <2%	≤5 cm-thick, irregularly-banded, alternating silicate-rich (grunerite + actinolite ± augite ± magnetite) and quartz-rich laminae
Jaspilite	x 0–10%	x 5–15%				x 75–90%	x 0–1%	x 0–5%	x <2%	Massive to coarsely-banded rock: fine quartz and calcite, with truncated magnetite bands, cross-cutting quartz-hematite veinlets, and stilpnomelane

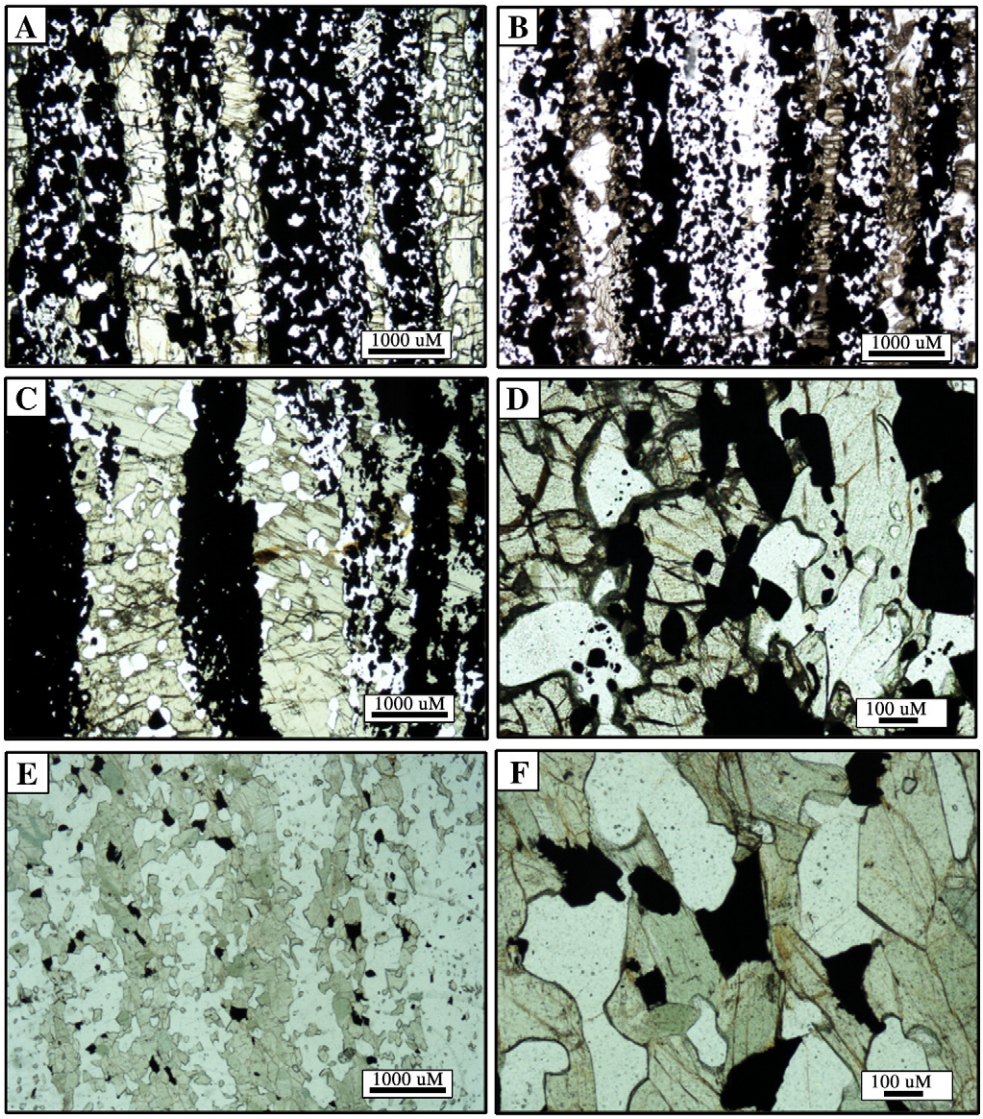

Fig. 5. Photomicrographs showing typical mineral grain relationships in the (A–D) BIF, and in the (E–F) banded silicate formation (BSF).

grunerite by reaction between carbonate and silica (section 5.1 in Dauphas et al., 2007a). In a number of BSF localities grunerite also coexists with Ca-amphibole, likely indicating an excess of Ca. This coexistence is better explained as a result of the following reaction between ferrodolomite and quartz to form actinolite–tremolite and cummingtonite–grunerite [reaction 3]:

$$14Ca(Mg_{0.5}Fe_{0.5})(CO_3)_2 + 16SiO_2 + 2H_2O \rightarrow Ca_2Mg_5Si_8O_{22}(OH)_2 + Fe_7Si_8O_{22}(OH)_2 + 14(Ca_{0.9}Mg_{0.1})CO_3 + 14CO_2. \quad (3)$$

Likewise, augite is possibly the result of a decarbonation reaction, and reinforces the idea that carbonates were present in the original sediment [reaction 4]:

$$Ca(Fe, Mg)(CO_3)_2 + 2SiO_2 \rightarrow Ca(Fe, Mg)Si_2O_6 + 2CO_2. \quad (4)$$

Minnesotaite and Fe-bearing carbonates (siderite, ankerite, ferroan dolomite) are common components in younger and less metamorphosed BIF successions and would suggest that the precursor mineral assemblages were similar.

Overall, petrographic data of the BIF and BSF show mineral assemblages corresponding to the upper-amphibolite facies of metamorphism (i.e., 500–650 °C, Klein, 2005). The first occurrence of actinolite in metamorphosed BIF coincides with the appearance of garnet in quartz–biotite schists at the upper-greenschist to epidote amphibolite facies (e.g., James, 1955; Haase, 1982), which occurs at temperatures of around 450 °C (Bucher and Frey, 2002). Similar paragenesis to that present in the Nuvvuagittuq banded formations were reported for the Negaunee Iron Formation, zones 2 and 3(a) of the Marquette District (Michigan, USA), with estimated temperatures between 500 and 600 °C (Haase, 1982). Furthermore, these minerals are similarly well-represented in the BIF of the 3.8 Ga Isua Supracrustal Belt whose assemblages are also compatible with amphibolite-facies P–T conditions (Dymek and Klein, 1988). Petrological studies of the Nuvvuagittuq amphibolites also show that they have all been affected by an intense regional amphibolite facies metamorphism. This observation coincides with the highest temperatures obtained by means of the garnet–biotite geothermometer on the least altered biotite, which ranges from 550 to 640 °C (O'Neil et al., 2007; Cates and Mojzsis, 2009).

Based on the progression from chlorite–epidote greenstones to garnet-free amphibolites and to garnet-bearing amphibolites, O'Neil et al. (2007) suggested a map-scale metamorphic gradient from upper greenschist in the west to upper amphibolite facies in the east of the NSB. Virtually the same mineral assemblages found in the BIF and BSF

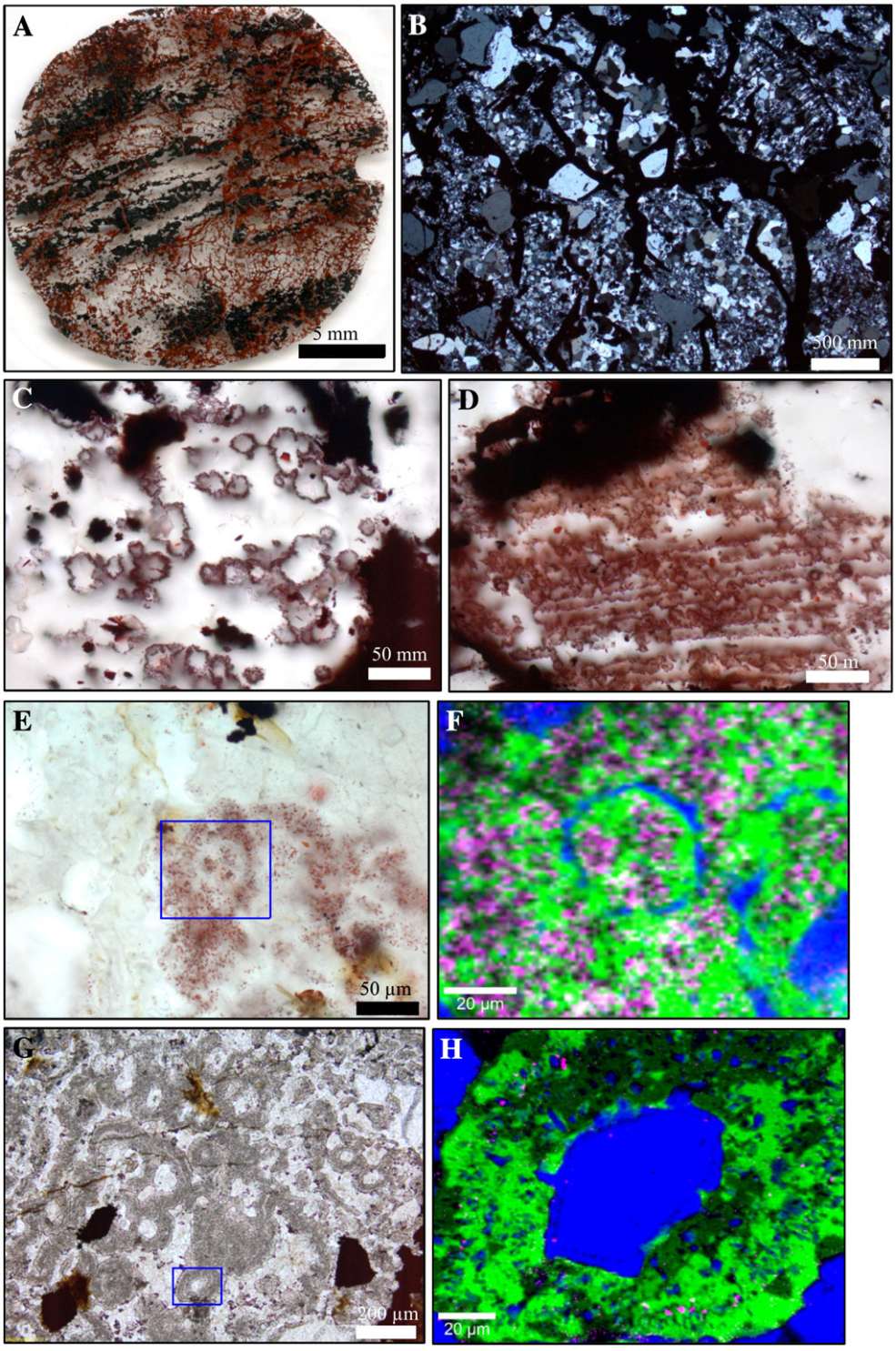

Fig. 6. Photomicrographs (A, C–E, G) and Raman spectroscopy images (F, H) of jaspilite in thin section.

occur sporadically at several localities. Although some slight differences can be seen, such patterns of occurrence appear to be a function of localized variations in rock bulk composition and fluid phase composition rather than of the regional metamorphic gradient. For instance, Fig. 7 shows the range of amphibole and pyroxene compositions. The presence of ripidolite, which was found in only two actinolite-bearing BSF samples, might indicate retrogression. However, it does not rim the amphibole, but instead occurs as small fans and sheaves. In the associated garnet-bearing cummingtonite-amphibolite, chlorite has been observed as inclusions in the garnet and appears to be part of the high-temperature metamorphic assemblage. In other cases, chlorite exists outside the garnet and there is no clear-cut textural evidence that the chlorite is secondary. When biotite is present, however, it is altered to chlorite, indicating the existence of extensive retrograde metamorphic effects (O'Neil et al., 2007). Therefore, it is possible that chlorite is part of both, the high-temperature assemblage and of retrograde origin.

The mineralogy of the jaspilite and crystallinity of quartz in this sub-type points to lower metamorphic grades than for BIF and BSF,

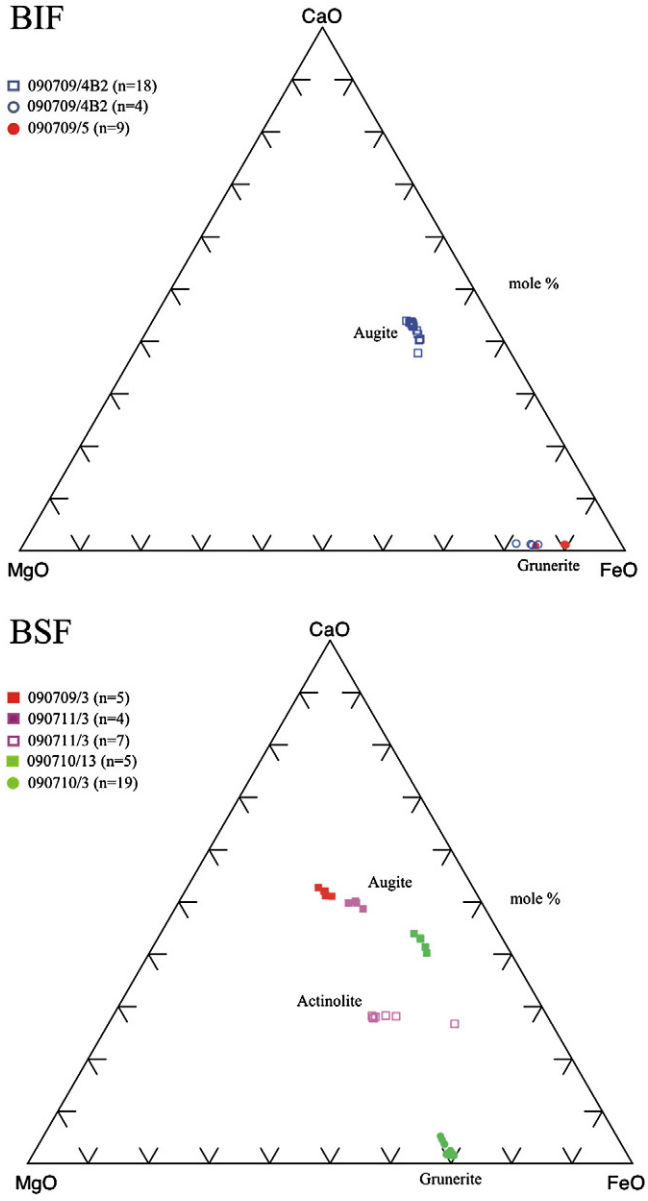

Fig. 7. Ternary diagrams showing the chemical composition of amphiboles and pyroxenes in the NSB BIF and BSF units in terms of molecular percentages of MgO, SiO and FeO.

which is consistent with previous observations (O'Neil et al., 2007). While the presence of acicular stilpnomelane in the jaspilite indicates retrograde metamorphism at the lower greenschist facies, the absence of amphibole suggests that these rocks did not reach the amphibolite facies as seen in the rest of the Nuvvuagittuq Supracrustal Belt. In addition, the presence of fine-grained rounded calcite structures with micron-size flaky hematite inclusions (Fig. 6E–H) suggests that diagenetic concretionary structures have been preserved in jaspilites. This is proposed because these structures are similar to rounded carbonate structures generated from the oxidation of organic matter by ferric oxides during diagenetic experiments simulating the formation of BIF (Koehler et al., 2009).

5. Whole-rock composition of the BIF

The BIFs consist predominantly of SiO_2 (33–63 wt.%) and Fe_2O_{3total} (32–66 wt.%). The Fe_2O_{3total} content is particularly high when compared to other Eoarchean (and younger) BIF (Klein, 2005), a feature presumably due to remobilization and concentration of Fe during the polyphase high-grade metamorphism. MgO abundances are <4 wt.%, while the remainder of the other major elements, including Al_2O_3, are generally <1 wt.%. Sulfide grains were purposely avoided during sampling and so S abundances are all <0.3 wt.%. In terms of trace metals, the most abundant are Ni and Zn, while incompatible elements and Y tend to be low, on average: Hf and Th (0.3 ppm); Zr (2 ppm), and Y (9 ppm) (Fig. 8; see Mloszewska et al., 2012, supplementary data table 1). REE + Y profiles (Fig. 9) show distinct seawater-like anomalies: positive La ($La/La^* = 1.73 \pm 0.34$), positive Eu ($Eu/Eu^* = 2.21 \pm 0.44$), super-chondritic Y/Ho ratios ($Y/Ho = 33.82 \pm 2$), and LREE<MREE<HREE ($Pr/Yb_{SN} = 0.16 \pm 0.17$; $La/Yb_{SN} = 0.47 \pm 0.27$).

5.1. Whole-rock composition of the BSF

These rocks show the greatest variability in major elements: Fe_2O_3 (2 to 55 wt.%), SiO_2 (28–90 wt.%), Al_2O_3 (generally <1 wt.%), CaO (3 to 16 wt.%), and MgO (2 to 12 wt.%). Like in the BIF, sulfide grains were purposely avoided, and so S abundances were low (<0.6 wt.%). Similarly, the most abundant trace metals are Ni and Zn (see Mloszewska et al., 2012, supplementary data table 1). The following incompatible elements are especially low: Hf and Th (<0.5); Zr (<3 ppm), and Y (<5 ppm). All other trace elements tend to be <15 ppm (Fig. 8). The REE + Y profiles of the BSF (Fig. 9) also tend to show seawater-like anomalies: positive La ($La/La^* = 2.31 \pm 1$), positive Eu ($Eu/Eu^* = 1.84 \pm 0.16$), super-chondritic Y/Ho ratios ($Y/Ho = 37.40 \pm 6.83$), and LREE<MREE<HREE ($Pr/Yb_{SN} = 0.30 \pm 0.19$; $La/Yb_{SN} = 0.70 \pm 0.23$).

5.2. Mineral composition

The compositions of mineral phases were analyzed in a subset of BIF and BSF samples (Fig. 10), but not in the jaspilite.

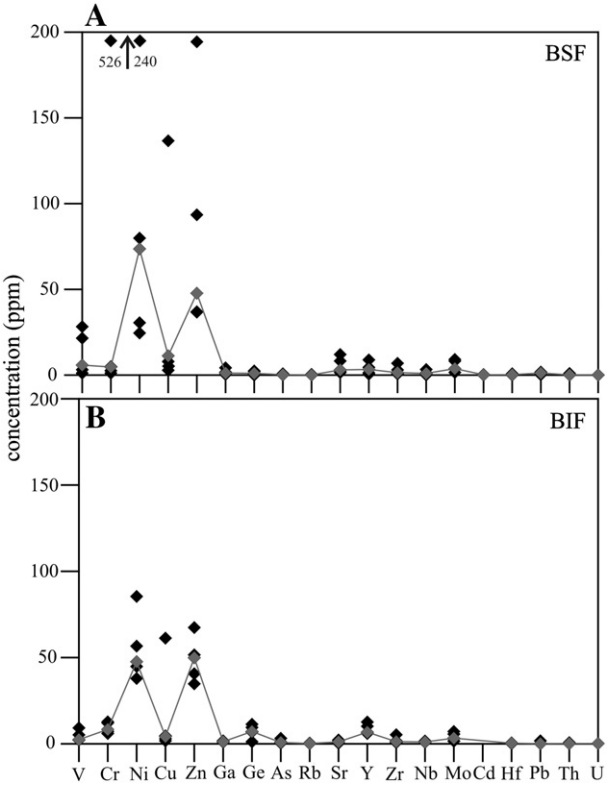

Fig. 8. Whole-rock trace element abundances (ppm) in the (A) BIF and the (B) BSF. See Mloszewska et al. (2012) for source data and methodology.

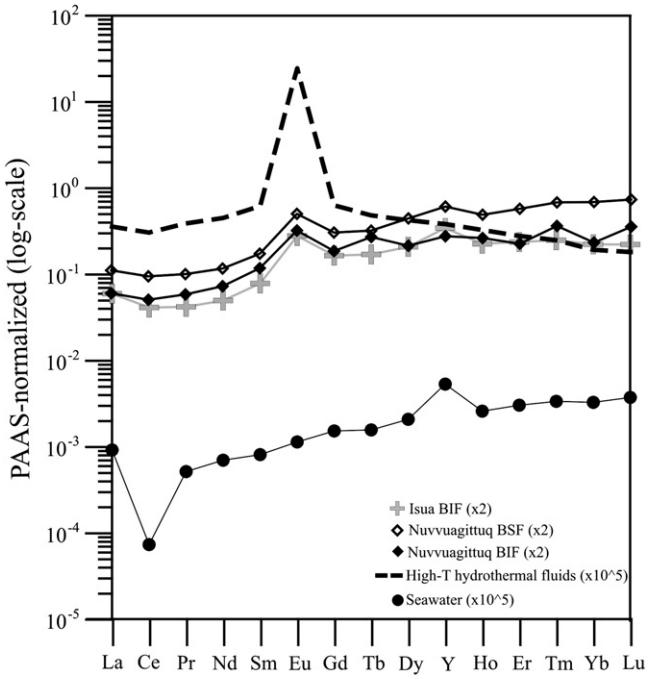

Fig. 9. REE + Y distribution in the NSB BIF and BSF, as well as average high temperature (>350 °C) hydrothermal fluids, modern pacific seawater, and BIF from the ca. 3800 Ma Isua Supracrustal Belt (Alibo and Nozaki, 1999; Bau and Dulski, 1999; Bolhar et al., 2004). After Alexander et al. (2008).

5.2.1. Magnetite

Apart from being overwhelmingly Fe-rich (FeO_{total} = 93 wt.%), magnetite has insignificant abundances of the other major elements (Na_2O, K_2O, Al_2O_3, MnO, CaO, MgO, P_2O_5, SiO_2,TiO_2). There is a negative linear correlation between iron and aluminum ($r^2 = 0.8$) suggesting the substitution of aluminum for iron in the magnetite structure. In terms of trace elements, Ni (100 ppm) and Zn (69 ppm) occur in the highest abundances. Additionally, magnetite in the BIF has notable abundances of Cr (30 ppm), Ge (27 ppm) and Co (13 ppm), while BSF magnetite has notable abundances of V (52 ppm) and Ga (13 ppm). The rest of the trace elements tend to occur in abundances < 10 ppm.

5.2.2. Quartz

Quartz is ~99 wt.% SiO_2 while the rest of the major elements occur in concentrations < 0.2 wt.%. Zn (76 ppm) and Ni (39 ppm) occur in the highest concentrations, followed by Cu (20 ppm) and Cr (17 ppm), while all others occur in concentrations < 10 ppm. Quartz composition appears fairly uniform between rock types.

5.2.3. Grunerite

The SiO_2 content is relatively constant in both BIF and BSF (SiO_2 ~ 51 wt.%); Fe is higher in the former (FeO_{total} BIF ~ 44 wt.% vs. calc-silicate ~30 wt.%); Mg is higher in the BSF (MgO ~ 13 wt.% vs. 5 wt.%). All other major element concentrations tend to be <1 wt.%. A positive linear correlation exists between Mn and Mg ($r^2 = 0.8$), suggesting substitution of Mn for Fe in the crystal structure. Similar to magnetite, Ni (60 ppm) and Zn (170 ppm) occur in the highest abundances. Co also occurs in notable concentrations in both rock types, but is significantly more abundant in the BSF (32 ppm) compared with the BIF (16 ppm). Additionally Ge occurs in notable concentrations in the BIF (16 ppm), while the rest of the trace elements tend to be <10 ppm.

5.2.4. Augite

Augite is dominantly composed of SiO_2 (51 wt.%), CaO (22 wt.%), and FeO, where BIF augite is higher in Fe than the calc-silicate augite (21 wt.% vs. 12 wt.%). MgO also occurs in notable abundances, but is higher in the BSF augite (11 wt.% vs. 7 wt.%). The rest of the major elements tend to be <0.5 wt.%. Fitting with the overall trend, Ni (51 ppm) and Zn (142 ppm) occur in the highest abundances, followed by Sc (34 ppm). Ni and Cr tend to be more variable in BSF augite sometimes reaching up to 477 ppm and ≤1000 ppm, respectively, in some grains, while in most samples, Cr tends to be below the detection limit. Additionally, in the BIF, Sr (58 ppm) and Ge (21 ppm) occur in notable concentrations, while in the BSF, Co (51 ppm) and V (59 ppm) are high. Y in augite tends to vary significantly between samples of both rock types ranging from 5 to 87 ppm.

5.2.5. Actinolite

Actinolite shows average compositions of SiO_2 (53 wt.%), FeO_{total} (20 wt.%), and CaO (13 wt.%), and MgO (12 wt.%). Mg and Fe show strong negative linear correlation emphasizing the substitution of Mg for Fe in the crystal structure. In terms of trace elements, Zn (362 ppm), Ni (77 ppm), Y (38 ppm), Sc (36 ppm), and V (41 ppm) occur in notable concentrations.

5.3. Iron isotope composition

Low temperature aqueous and biochemical processes can impart large fractionations to iron isotopes in sediments (e.g., Dauphas and Rouxel, 2006; Johnson et al., 2008). The mechanisms that are relevant to BIF are oxidation of Fe(II) dissolved in seawater and redox cycling after sediment deposition. Several biogeochemical pathways have been considered to explain the oxidation of Fe(II) into Fe(III) and the subsequent precipitation of insoluble ferric oxyhydroxides (e.g., ferrihydrite) in an environment that was globally anoxic: (1) oxygenic photosynthesis could have created oases of O_2 in the photic zone that induced iron oxidation and precipitation (Cloud, 1973), (2) bacteria could have directly used $Fe(II)_{aq}$ as an electron donor during anoxygenic photosynthesis, thus coupling carbon fixation to iron oxidation (Widdel et al., 1993), or (3) with no ozone, the atmosphere may have been transparent to UV photons that could have induced iron photo-oxidation in the upper-layers of the ocean (Cairns-Smith, 1978). Direct oxidation and anoxygenic photosynthesis have been studied in laboratory and field settings and these processes tend to enrich Fe(III) in the heavy isotopes relative to Fe(II) (e.g., Bullen et al., 2001; Croal et al., 2004). The main controlling factor seems to be equilibrium isotope fractionation between Fe(II) and Fe(III), which can impart a fractionation of up to ~+3‰ in $\delta^{56}Fe$ (Welch et al., 2003). However, photo-oxidation pathways have not yet been studied in detail for their effects on iron isotopes and some of the discussion below may need to be re-evaluated in light of future experiments.

Iron oxides in BIF tend to have heavy iron isotopic compositions relative to other minerals, consistent with the view that Fe(III) in BIF was derived from partial oxidation of $Fe(II)_{aq}$ in seawater (Dauphas et al., 2004; Planavsky et al., 2011). Bulk Eoarchean BIFs from Isua have among the heaviest iron isotopic compositions among BIFs of all ages (Dauphas et al., 2004, 2007a). This is best explained if the oxidation was partial (<50%), meaning that the oxidative capacity at that time was insufficient to process all $Fe(II)_{aq}$ available. This heavy iron isotopic composition was used to ascertain the chemical sedimentary nature of the protolith of banded quartz–pyroxene rocks from Akilia (Dauphas et al., 2004; also see Manning et al., 2006 for independent arguments pertaining to this question). The heavy iron isotopic compositions and high Fe/Ti ratios of quartz–pyroxene rocks from Akilia indicate that these rocks are genuine chemical sedimentary rocks, and are probably not products of metasomatism as was advocated by Fedo and Whitehouse (2002).

Iron isotopes in BIF have also proven to be extremely useful at identifying the biogeochemical processes that affected these sediments after deposition. In particular, iron isotopes have played an

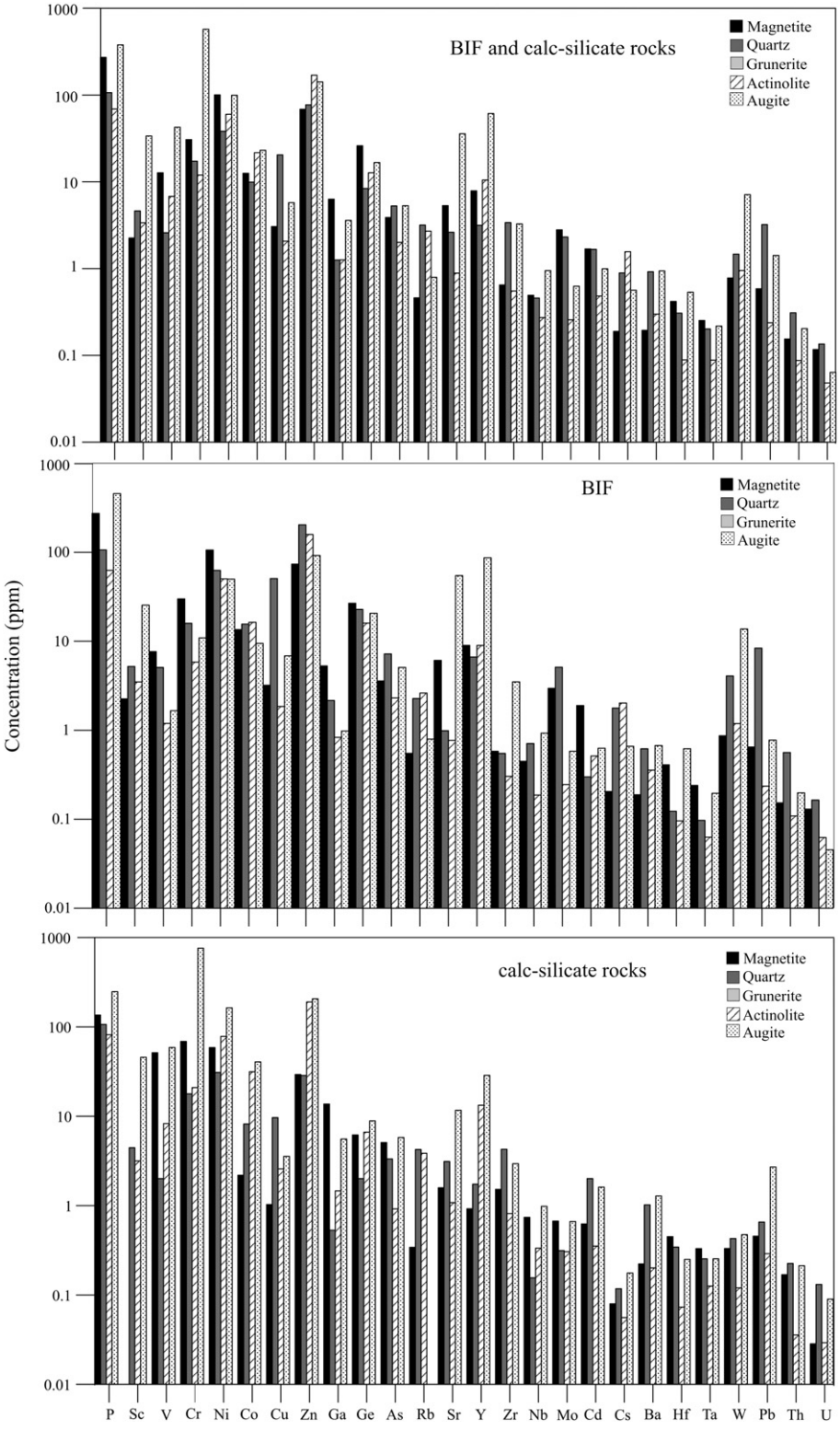

Fig. 10. Trace elements present in specific mineral phases in the BIF and BSF units.
See Mloszewska et al. (2012) for source data and methodology.

important role in identifying dissimilatory iron reduction (DIR), a mode of bacterial respiration that uses Fe(III) instead of O_2 as the electron acceptor. Beard et al. (1999) first documented the isotopic fractionation associated with DIR and found that dissolved $Fe(II)_{aq}$ produced by such biological activity had light iron isotopic composition relative to solid ferric oxyhydroxides. This observation was confirmed by several subsequent experiments. For instance, Johnson et al. (2003) measured the iron isotopic composition of mineral separates from BIF and they argued for the presence of DIR in these rocks. More definitive evidence was provided by the studies of Heimann et al. (2010), and Craddock and Dauphas (2011), who studied the C and Fe isotopic compositions of coexisting iron-oxides

and carbonates in well-preserved Neoarchean/Paleoproterozoic BIFs from western Australia and South Africa. Iron-poor carbonates tend to have lower δ^{56}Fe and higher δ^{13}C than iron-rich carbonates. This is readily explained by DIR; bacterial respiration oxidizes organic matter with low δ^{13}C values using ferric oxyhydroxides with high δ^{56}Fe, releasing CO_2 and $Fe(II)_{aq}$ in the pore-water that can subsequently form iron-rich carbonates. Craddock and Dauphas (2011) found similar C–Fe isotope systematics in carbonates from Isua and argued that DIR was active as early as 3.75 Ga. Thus, most iron-rich carbonates may have a diagenetic origin and their presence cannot easily be used to argue for or against a high pCO_2-atmosphere (see Rosing et al., 2010; Dauphas and Kasting, 2011 for alternate views).

It was found that the iron isotopic compositions of chemical sedimentary rocks from Nuvvuagittuq are similar to those documented in Isua and Akilia (O'Neil et al., 2007; Dauphas et al., 2007a, 2007b). Fig. 11 shows a false color X-ray mosaic of a relatively well-preserved BIF from Nuvvuagittuq (IN05007). It is composed of parallel bands of magnetite intercalated with grunerite/cummingtonite and quartz. Pyrite is disseminated in magnetite layers and a vein of calcite and ankerite cross-cuts the sample in the upper-left corner. The iron isotopic compositions of the different magnetite layers were analyzed and revealed homogeneous δ^{56}Fe values (0.58 ± 0.04‰; Dauphas et al., 2007a). More recent and better-preserved BIFs tend to show some heterogeneity from layer to layer in their iron isotopic composition (e.g., Steinhoefel et al., 2010). Most likely, the amphibolite-facies metamorphism that affected these rocks homogenized the iron isotopic composition at the scale of a hand-specimen and inter-mineral isotope variations reflect equilibrium isotopic fractionation during metamorphism. Whitehouse and Fedo (2007) reported large (2‰) microscale heterogeneity of iron isotopic composition in BIF from Isua by high-resolution ion microprobe, which they interpreted to be an inherited diagenetic signature. This result is unexpected given the high metamorphic grade of these rocks and the contradictory results of Dauphas et al. (2007a, 2007b). A more likely interpretation is that it reflects an analytical artifact arising from the fact that iron isotope analysis of magnetite by ion microprobe is affected by crystal orientation (Kita et al., 2011), which was not addressed in the origin study of Whitehouse and Fedo (2007).

Many chemical sedimentary rocks from Nuvvuagittuq have heavy iron isotopic composition (~+0.5 to +0.8‰ in δ^{56}Fe) and high Fe/Ti ratios. This is entirely consistent with derivation of these rocks by partial oxidation of Fe(II) in seawater. A notable feature of iron isotope systematics in chemical sedimentary rocks from Nuvvuagittuq is that some have iron isotopic compositions close to seawater. These samples also have high Mg/Fe, Ca/Fe, and Mn/Fe and must derive from a carbonate-silica protolith (Fig. 12). As discussed previously, iron-poor carbonates formed by precipitation from seawater tend to have light iron isotopic compositions. Reaction of these carbonates with excess silica during amphibolite-facies metamorphism will produce the mineral paragenesis (cummingtonite + actinolite + quartz) that is observed in some chemical sedimentary rocks from Nuvvuagittuq. Overall, the iron isotope signatures measured in Nuvvuagittuq chemical sedimentary rocks are very reminiscent of the signatures measured in Isua. With that said, the database of iron isotope measurements is limited and further work is required to document the stable isotope variations in chemical sedimentary rocks from this locality and to understand how these signatures reflect mineral precipitation and biogeochemical reworking during paragenesis.

5.4. Carbon isotope compositions

Carbonate has been detected in a few BIFs and was measured to have a $\delta^{13}C_{carb}$ value of −2.2‰ and $\delta^{18}O_{carb}$ value of −16.1‰, whereas carbonates in jaspilite have $\delta^{13}C_{carb}$ values between −4.3 and −6.1‰

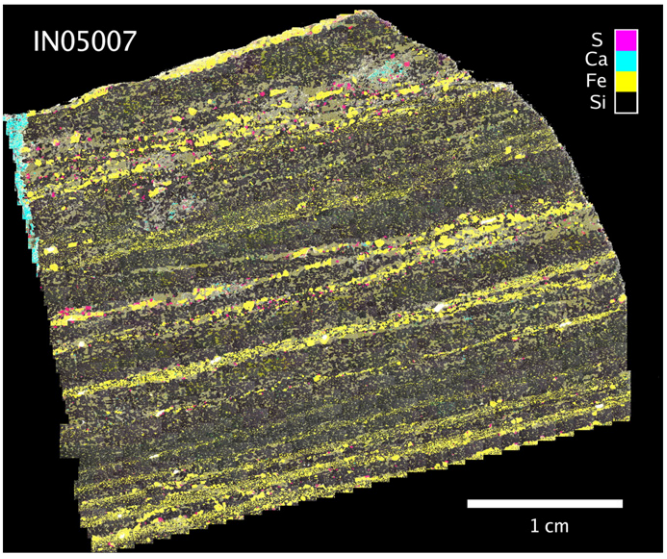

Fig. 11. False X-ray mosaic image assembled from 4 × 1000 frames. Ca = cyan; S = magenta; Fe = yellow; Si = black. Magnetite (yellow) layers alternate with cummingtonite–grunerite (light dark yellow-gray) and quartz (dark gray) layers, and vein consisting of calcite and ankerite crosscuts the layering at the top left corner, in cyan. Disseminated pyrite (magenta) occurs mainly in the magnetite layers, and actinolite associated with the cummingtonite–grunerite occurs as small domains (green-gray).
After Dauphas et al. (2007b).

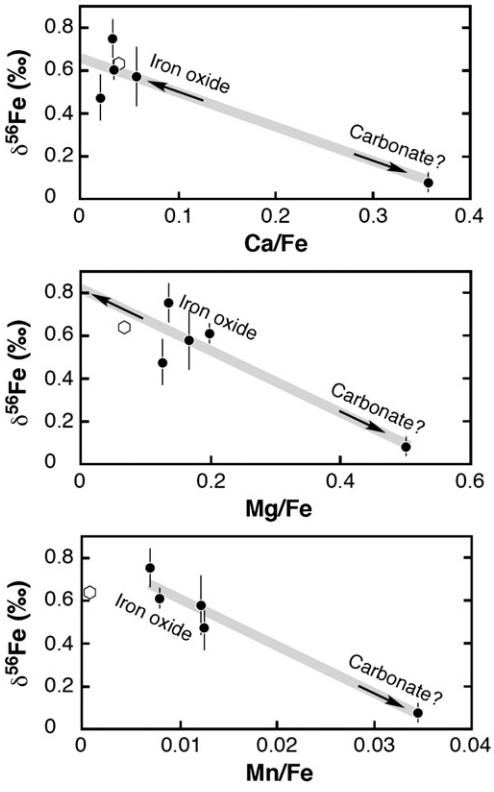

Fig. 12. Diagrams showing binary mixing between hypothetical Fe-oxide (Fe-ox) and carbonate (carb) end-members. Filled symbols represent measurements of quartz ± magnetite ± amphibole/pyroxene rocks from NSB, while empty ones represent composition of the BIF geostandard IF-G from the Isua Supracrustal Belt in southern West Greenland (Dauphas et al., 2004; Govindaraju, 1994). An initial composition of 0.3–0.4‰ for an Fe-oxide end-member of the NSB BIF, upon extrapolating the trends to zero for Ca/Fe or Mg/Fe.
After Dauphas et al. (2007b).

and $\delta^{18}O_{carb}$ values between −19.1 and −16.6‰ (Papineau et al., 2011). These isotope compositions are consistent with metamorphic devolatilization (Valley, 1986a, 1986b). Whole-rock samples of Nuvvuagittuq BIF contain low levels of organic carbon between 0.034 and 0.004 wt.% and a range of $\delta^{13}C_{org}$ values between −26.8 and −18.2‰. Similarly, jaspilites also have low levels of organic carbon between 0.034 and 0.004 wt.% and a range of $\delta^{13}C_{org}$ values between −24.6 and −21.1‰ (Papineau et al., 2011). While these carbon isotope compositions might be consistent with a biological origin, a number of abiotic pathways are also capable of synthesizing reduced carbon compounds (e.g., Fischer–Tropsch type synthesis) after metamorphic overprinting (the reader is referred to a review on isotope biosignatures in ancient rocks by Horita, 2005, and references therein). In addition, before any determination on the origins of this carbonaceous material can be made, it is crucial to establish an indigenous origin to the carbonaceous material. This means that the carbonaceous material must demonstrably have undergone the same metamorphic history as the host rock.

Raman spectra and selected area electron diffraction patterns of micron-sized particles of poorly crystalline graphite associated with apatite from an NSB BIF point to a structure consistent with greenschist facies (retrograde) metamorphism that occurred after peak metamorphism of the chemical sedimentary rocks. Papineau et al. (2011) also observed that poorly crystalline graphite and apatite were associated with low-temperature fluid-deposited alteration minerals that include goethite, cronstedtite [$Fe^{2+}{}_2Fe^{3+}{}_2SiO_5(OH)_4$], chalcopyrite, and sphalerite. Collectively these observations point to a late fluid-deposition of poorly crystalline graphite, and demonstrate the limitation of bulk carbon isotope analyses, which cannot be used to discriminate against organic contamination from late hydrothermal or metamorphic fluids.

6. Implications for Eoarchean seawater composition

Seawater composition, as reflected in BIF, represents a mixture of both hydrothermal inputs (e.g., Dymek and Klein, 1988; Derry and Jacobsen, 1990; Danielson et al., 1992; Bau and Möller, 1993) and, in some cases, small amounts of detrital inputs (e.g., Ewers and Morris, 1981). Throughout geological history, the contribution of hydrothermal fluids to seawater composition has probably decreased substantially as mantle temperatures have decreased with time (e.g., McKenzie and Weiss, 1975), whereas the relative contribution of detrital material to seawater reflects, at least in part, the rate and intensity of erosional processes as the volume of exposed continental crust has increased with time (e.g., Kump and Barley, 2007). In the case of the latter, because detrital material contains significant amounts of metals and other elements relative to seawater, it tends to obscure seawater signals, thus the use of BIF as potential seawater proxies is conditional upon them containing insignificant amounts of detritus. The composition of the Nuvvuagittuq BIF and BSF suggests low detrital contents, with Al_2O_3 generally <1 wt.%, TiO_2<0.2 wt.%, and low Zr (<10 ppm). REE + Y abundances in both these units are also correspondingly low (Fig. 9), and are comparable to those of other BIF from the Isua Supracrustal Belt (e.g., Dymek and Klein, 1988; Bolhar et al., 2004). REE + Y profiles of the BIF and the BSF show distinct, seawater-like anomalies (depleted LREE, positive La and Eu anomalies, and superchondritic Y/Ho ratios). Because of their variable oxidation states, Ce and Eu are the most mobile of the REE. Europium is sensitive to post-depositional changes, such as reducing conditions during diagenesis, and high temperatures associated with metamorphic disturbances (Bilal, 1991; MacRae et al., 1992), while Ce is sensitive to changes in redox conditions (Bau, 1999). The NSB chemical sediments lack significant negative Ce anomalies (see fig. 7 in Mloszewska et al., 2012), similar to other Archean and Paleoproterozoic BIFs (Bau and Dulski, 1999; Bolhar et al., 2004; O'Neil et al., 2007; Planavsky et al., 2010a). The consistently positive Eu anomalies relative to neighboring elements would suggest a primary feature of the rock, and is consistent with the high-temperature hydrothermal fluid contribution in the Archean oceans (e.g., Bau and Möller, 1993; Polat and Frei, 2005; Frei and Polat, 2007). Just how much of a contribution depends on the relative location of the BIF depositional basin and the hydrothermal system, as well as the age of the BIF. Although there are few studies which have explicitly looked at ascertaining the amount of hydrothermal versus continental input for BIF, Alexander et al. (2008) used a simple 2-component mixing model between Eu/Sm and Sm/Yb in the ca. 2900 Ma Pongola Supergroup in South Africa to determine the degree of hydrothermal contribution to seawater as represented in BIF; they suggested that the hydrothermal contribution to Eoarchean seawater at that time was around 0.1% (Alexander et al., 2008).

The mobility of trace metals during BIF metamorphism is of particular importance for the use of BIF as potential ancient seawater proxies. Ni and Zn occur in the highest abundances in the Nuvvuagittuq BIF and BSF; they were found to be especially associated with the Fe–Mg silicate mineral phases and secondarily the magnetite (Mloszewska et al., 2012). Sulfide minerals (e.g. pyrite) occur in the NSB BIF but samples with low S abundances were selected, and S had no obvious relationship with Ni and Zn concentrations. Fe-oxide minerals have an affinity for sorbing metals such as zinc, where Dyer et al. (2004) found that at circum-neutral pH conditions, the sorption capacity of two-line ferrihydrite (thought to be one of the precursors to the Fe-oxide minerals in BIF today) for Zn(II) is 0.46 mol per mol of Fe(II). Similarly, ferrihydrite also has a high sorption capacity for Ni(II) (Konhauser et al., 2009), so much so that ferrihydrite is a controlling factor for Ni bioavailability in modern environments (Trivedi and Axe, 2001; Xu et al., 2007). As yet, little is known about the post-depositional mobility of trace metals between the mineral phases in BIF, and so it is plausible that these metals were remobilized within the BIF itself and re-sorbed onto different mineral phases during metamorphism.

Nickel is a signature nutrient for methanogens, occurring as a metal cofactor in two primary enzymes involved in the production of methane, as well as in the enzyme CO-dehydrogenase which reduces CO_2 to CO in acetogenic methanogenic bacteria; it is also used by non-methanogens in urease and some dehydrogenases (Ragsdale and Kumar, 1996; daSilva and Williams, 2001). Nickel was abundant in Archean seawater, and it is thought to have reached abundances of up to 400 nM, but by 2500 Ma, it appears to have dropped to below 200 nM, and decreased steadily to modern seawater values of 9 nM by around 550 Ma (Konhauser et al., 2009). The cause of this decrease is attributed to a decline in mantle temperatures, and a subsequent decrease in the eruption of Ni-rich ultramafic mantle rocks such as komatiites (Barley et al., 1998; Campbell and Griffiths, 1992; Isley and Abbott, 1999; Barley et al., 2005). An indirect consequence of this decrease in seawater Ni is thought to have been the Great Oxidation Event at ca. 2.4 Ga (Holland, 2002; Bekker et al., 2004; Canfield, 2005; Holland, 2009; but cf. ; Law and Phillips, 2006; Ohmoto et al., 2006; Kerrich et al., in press), where a decrease in the production of methane by methanogenic bacteria allowed for the proliferation of oxygen-producing cyanobacteria (Konhauser et al., 2009). That O_2 then scrubbed methane from the atmosphere (Zahnle, 2006). Experimentally-derived partitioning coefficient between Ni and ferrihydrite applied to Ni abundances in the Nuvvuagittuq BIF suggests abundances of up to around 300 nM in the Nuvvuagittuq depositional basin, which correlates well with the above findings (Mloszewska et al., 2012).

Zn in modern seawater is relatively low, with an average of around 9 nM (Bruland and Lohan, 2004), and is largely sourced by mafic and ultramafic volcanic rocks (Le Roux et al., 2010). The evolution of Zn in seawater through time has been the subject of recent discussion, because of the importance of Zn in eukaryotic metalloenzymes. Zn is a defining feature of the Eukaryote metallome, while *Bacteria* and *Archaea* have

few exclusive Zn containing enzymes (typically for gene transcription and translation), and can substitute other elements with similar ionic radii (e.g., Co) for Zn in others (daSilva and Williams, 2001). It was proposed that seawater Zn abundances increased to present-day values during the Neoproterozoic when deep-sea oxygenation allowed Zn^{2+} to diffuse throughout the water column; until then, higher Zn values only existed in coastal pockets of oxygenated waters (Saito et al., 2003). By contrast, dissolved sulfide has a high affinity for Zn, and it has been argued that even low concentrations of sulfide, as in Archean seawater where HS^{-} <1 mM would have complexed most Zn into non-bioavailable Zn–sulfide complexes (Saito et al., 2003). This seems to correlate with findings based on proteomic sequencing suggesting that many Eukaryote Zn-binding proteins didn't evolve until the Mesoproterozoic or later, in an oxic environment (Dupont et al., 2010). In contrast, recent evidence in black shales through time suggests that seawater Zn abundances did not change significantly contrary to the above suggestions (Scott et al., in press). This finding is corroborated by seawater Zn abundances derived from the Nuvvuagittuq BIF through the application of an experimentally derived partitioning coefficient, suggesting that in the Nuvvuagittuq depositional basin, they were closer to modern day values at 20 nM, and conservatively, a biologically significant 0.7 nM would remain uncomplexed as Zn^{2+} (Mloszewska et al., 2012). In this regard, further inquiry into reconciling the proteomic and rock records will have to be done.

6.1. The Nuvvuagittuq depositional environment

All metamorphic rocks have igneous or sedimentary protoliths that can be explained based on observations of contemporary systems and well-preserved ancient archetypes. The geochemistry of these protoliths governs the gross compositions of the metamorphic products, and we propose to use this information to compose a self-consistent geologic setting for the compositional origin of the NSB sediments. The picture that emerges is of a marine environment with occasional volcaniclastic input associated with mixed mafic- and felsic-hosted hydrothermal systems, voluminous exhalative volcanism, volcanic arc-related processing, and the deposition of chemical as well as infrequent detrital sediments.

The rock-types of all known Eoarchean, supracrustal volcano-sedimentary successions are dominated by massive to foliated, amphibolitized mafic and ultramafic hornblende + plagioclase rocks. These tend to range in composition from basalts and basaltic-komatiites, to basaltic-andesites and dacites. A feature that sets the Nuvvuagittuq belt apart from other Eoarchean supracrustals (e.g. Isua) is that dominant amphibolites are a CaO-poor (cummingtonite-rich) variety. This chemical feature has been ascribed a post-depositional origin (O'Neil et al., 2007, 2011), possibly from albitization of the cummingtonite-amphibolite protolith by hot hydrothermal fluids at time of formation (Cates et al., in press). Alternatively, the reaction of carbonate with silica in amphibolite facies metamorphism of a rock depleted in calcium can lead to cummingtonite, especially in sedimentary protoliths or rocks with a significant sedimentary component (Klein, 1973).

6.1.1. Structural controls on sedimentation

The nature of tectonic regimes in the Archean remains a matter of debate (e.g., Kerrich and Polat, 2006). Numerous arguments have been raised concerning the enhanced thermal regime and associated differences in the mechanical behavior of the lithosphere, that either hindered or facilitated plate tectonics at the earliest times (Korenaga, 2011). Thus, caution is warranted in presenting any interpretative sketches of the structural basis and sedimentary deposition for the Nuvvuagittuq basin. The Nuvvuagittuq rocks can be understood in the context of ocean floor volcano-sedimentary processes associated with crustal thickening and mixed felsic- and mafic-hosted hydrothermal systems in a rapidly evolving submarine environment (the transition from an oceanic plateau to an arc, e.g., O'Neil et al., 2011). Such scenarios are common in contemporary intra-oceanic crustal settings at ocean–ocean plate boundaries (e.g., Elliott et al., 1997), and can thus serve as a guide in our interpretation. Under progressive formation of lava piles in arc and back-arc basins, hydrothermal alteration of seafloor and (mafic) volcanic detritus accompanies deposition of ferruginous sediments and the intrusion of felsic igneous rocks such as is observed in the Manus (Binns et al., 2002; Lackschewitz et al., 2004) and Lau (Hahm et al., 2012) basins of the southwest Pacific. At those back-arc basin sites, hydrothermal vent fluids have REE patterns (Douville et al., 1999) quite similar to the NSB BIF and BSF, and the igneous rocks range in composition from basaltic-picritic to dacitic.

6.1.2. A submarine, potentially felsic-hosted volcano-sedimentary system

Several different meta-igneous rock types have been recognized in the NSB that, based on SiO_2, MgO and other contents, can be classified as basaltic-komatiite, basalt and basaltic-andesite. Relatively lower Sm–Nd values observed in some of the cummingtonite-amphibolite series compared with the higher Sm–Nd found in amphibolites from Isua and Akilia Association, suggest the influence of a felsic-hosted volcanic system. The high Eu/Eu* anomalies of the BIF suggest a strong high-temperature (>350 °C) hydrothermal component from a proximal hydrothermal fluid source. As previously noted (see Section 5.1), although the chemical sedimentary rocks also show an insignificant detrital component, the Nuvvuagittuq depositional basin seems to have had hiatuses in volcanism that were punctuated by a small fraction of detrital input as exemplified by the quartz–biotite schists and Cr-bearing quartzites (conglomerates and quartz sands, possibly representing "flysch" deposits; Cates et al., in press). The NSB outcrops mapped by Cates and Mojzsis (2007) and David et al. (2009) represent a deformed albeit preserved and interpretable Eoarchean volcano-sedimentary succession. The close proximity of hornblende- and cummingtonite-amphibolites and ultramafic units to rocks of sedimentary protolith such as chromite-bearing quartzites, quartz–magnetite–amphibole (±pyroxene) rocks (BIF), banded- to massive quartzites (BSF), and quartz–biotite schists (meta-conglomerate) comprise a coherent package traceable throughout most of the NSB (O'Neil et al., 2007). The succession of ultramafic flows, basaltic flows, chemical sedimentary precipitates and the occasional detrital lens or layer, is typical of ancient volcano-sedimentary series (e.g., Lowe and Byerly, 1999). Over time these become gradually invaded by granitoid sheets as the structural/tectonic regime of the oceanic crust hosting these volcano-sedimentary units continued to evolve (e.g., Petford, 1996).

7. Conclusion

The discovery of Eoarchean-aged sedimentary rocks in the Nuvvuagittuq Supracrustal Belt (NSB) has opened up new opportunities to further our knowledge of early hydrosphere–geosphere–biosphere systematics. The NSB chemical sedimentary rocks include an Fe-oxide rich unit (BIF), a Ca–Fe–Mg silicate rich unit (BSF), and jaspilite, an extension of the BIF in the southwest corner of the belt. The Fe-oxide rich and Fe–Mg silicate rich units possess the geochemical and petrographic characteristics of relatively detritus-free Archean chemical sedimentary rocks of BIF parentage, with minimal compositional changes due to remobilization outside these units. This suggests that they, at least partially, retain some of their seawater-like signature despite metamorphic overprinting (O'Neil et al., 2007; Dauphas et al., 2007a; Mloszewska et al., 2012). They are geochemically comparable to the quartz–magnetite BIF from Isua, and show similar petrography and metamorphic histories, which is the expected result for rocks of similar age and overall depositional setting. These characteristics suggest that they may be used as potential ancient seawater proxies. In this regard, the high seawater Ni abundances in the Nuvvuagittuq depositional basin (>300 nM)

corroborate with recent evidence suggesting that global Archean seawater was high in Ni (≤400 nM compared to modern average of 12 nM, Bruland and Lohan, 2004; Konhauser et al., 2009) due to the abundance of Ni-rich, Archean ultramafic rocks (komatiites), providing a vital nutrient for the methanogens that thrived in that eon. Seawater Zn abundances in the Nuvvuagittuq basin appear to have been comparable to modern values (≤20 nM versus modern average of 9 nM, Bruland and Lohan, 2004). Moreover, geochemical modeling suggests that even after complexing with Archean seawater sulfide complexes, a biologically significant portion of this would still remain uncomplexed (~0.7 nM), and would increase with higher Fe^{+2} abundances (Mloszewska et al., 2012). This further suggests that seawater Zn availability might not have played as significant a role in determining the timing of eukaryote evolution as interpreted by some studies (e.g., Saito et al., 2003; Dupont et al., 2010). This result is corroborated by recent findings on Zn in marine black shales through time (Scott et al., in press). More direct sources of potential biosignatures, such as graphite coatings on apatite grains in the NSB BIF, must be approached with caution, as their morphological and geochemical characteristics might have originated from post-depositional emplacement (Papineau et al., 2011). Importantly, the particular origins of such light carbon within these rocks must have originated from an even lighter source that has yet to be determined. Sulfur isotopes may also be a potential source of information on sulfur metabolisms preserved in the NSB rocks and further extensive investigations would certainly be of great benefit in this regard. In contrast, the NSB jaspilite appears to have been emplaced after the deposition of the cummingtonite-amphibolite unit, as jaspilite veins intrude into neighboring amphibolite units, and are associated with metacarbonate rocks emplaced by post-depositional fluid flow.

The lithological and geochemical similarity of the Nuvvuagittuq supracrustal units to those of the Isua Supracrustal Belt, and to the Akilia association of southern Greenland (Manning et al., 2006; Cates and Mojzsis, 2007; Cates and Mojzsis, 2006; Mloszewska et al., 2012) requires further careful investigation into the implications for shared geological histories or similar geological processes at different locations in the Eoarchean. While the meta-igneous rocks from the Eoarchean-aged Isua belt and Akilia association show positive μNd signatures which are explained by the incorporation of a pre-4300 Ma year old, depleted (high Sm/Nd) mantle source during its formation (Boyet et al., 2003; Caro et al., 2006; Bennett et al., 2007), the negative μNd signatures of the Nuvvuagittuq belt may instead suggest the incorporation of an ancient, low $^{142}Nd/^{144}Nd$, enriched component. The NSB is the best documented of several rafted supracrustal complexes that appear on maps of the Inuksuaq Complex generated by the Ministère des Resources Naturelles du Québec (Simard et al., 2003; Stevenson et al., 2006), and investigations of these other localities have the potential to provide further insights into global-scale Eoarchean environmental processes.

Acknowledgments

This work was supported by a National Sciences and Engineering Research Council of Canada award to KOK and an NSERC PGSD scholarship to AMM. SJM acknowledges support from the NASA Exobiology and Evolutionary Biology Program. Additional support to SJM came from NASA Lunar Science Institute, National Geographic Society, University of Colorado Office of the President, and the J. William. Fulbright Foundation. DP acknowledges support from the NASA Astrobiology Institute (grant no. NNA04CC09A), the NASA Exobiology and Evolutionary Biology Program (grant no. NNX08AO16G), the Carnegie Institution of Washington, the Carnegie of Canada, and Boston College. EP acknowledges the Agouron Institute for their support. We acknowledge Dr. M. Santosh, as well as Dr. Pat Eriksson and Dr. Rob Kerrich for their insightful comments.

References

Alexander, B.W., Bau, M., Andersson, P., Dulski, P., 2008. Continentally-derived solutes in shallow Archean seawater: rare earth element and Nd isotope evidence in iron formation from the 2.9 Ga Pongola Supergroup, South Africa. Geochimica et Cosmochimica Acta 72, 378–394.

Alibo, D.S., Nozaki, Y., 1999. Rare earth elements in seawater: particle association, shale-normalization, and Ce oxidation. Geochimica et Cosmochimica Acta 63, 363–372.

Anbar, A.D., Knoll, A.H., 2002. Proterozoic ocean chemistry and evolution: a bioinorganic bridge? Science 297, 1137–1142.

Barley, M.E., Krapez, B., Groves, D.I., Kerrich, R., 1998. The Late Archaean bonanza: metallogenic and environmental consequences of the interaction between mantle plumes, lithospheric tectonics and global cyclicity. Precambrian Research 91, 65–90.

Barley, M.E., Bekker, A., Krapež, B., 2005. Late Archean to Early Paleoproterozoic global tectonics, environmental change and the rise of atmospheric oxygen. Earth and Planetary Science Letters 238, 156–171.

Bau, M., 1999. Scavenging of dissolved yttrium and rare earths by precipitating iron oxyhydroxide: experimental evidence for Ce oxidation, Y-Ho fractionation, and lanthanide tetrad effect. Geochimica et Cosmochimica Acta 63, 67–77.

Bau, M., Dulski, P., 1999. Comparing yttrium and rare earths in hydrothermal fluids from the Mid-Atlantic Ridge: implications for Y and REE behaviour during near-vent mixing and for the Y/Ho ratio of Proterozoic seawater. Chemical Geology 155, 77–90.

Bau, M., Möller, P., 1993. Rare earth element systematics of the chemically precipitated component in early Precambrian iron formations and the evolution of the terrestrial atmosphere–hydrosphere–lithosphere system. Geochimica et Cosmochimica Acta 57, 2239–2249.

Beard, B.L., Johnson, C.M., Cox, L., Sun, H., Nealson, K.H., Aguilar, C., 1999. Iron isotope biosignatures. Science 285, 1889–1892.

Bekker, A., Holland, H.D., Wang, P.L., Rumble, D., Stein, H.J., Hannah, J.L., Coetzee, L.L., Beukes, N.J., 2004. Dating the rise of atmospheric oxygen. Nature 427, 117–120.

Bennett, V.C., Brandon, A.D., Nutman, A.P., 2007. Coupled ^{142}Nd–^{143}Nd isotopic evidence for Hadean mantle dynamics. Science 318, 1907–1910.

Bilal, B.A., 1991. Thermodynamic study of Eu^{3+}/Eu^{2+} redox reaction in aqueous solutions at elevated temperatures and pressures by means of cyclic voltammetry. Journal of Physical Sciences 46, 1108–1116.

Binns, R.A., Barriga, F.J.A.S., Miller, D.J., et al., 2002. Proceedings of the Ocean Drilling Program initial reports. Ocean Drilling Program. Texas A&M University, College Station, TX 77845-9547, USA.

Black, L.P., Sheraton, J.W., James, P.R., 1986. Late Archaean granites of the Napier Complex, Enderby Land, Antarctica: a comparison of Rb–Sr, Sm–Nd and U–Pb isotopic systematics in a complex terrain. Precambrian Research 32, 343–368.

Bleeker, W., 2004. Towards a 'natural' time scale for the Precambrian—a proposal. Lethaia 37, 219–222.

Boily, M., Leclair, A., Maurice, C., Bédard, J.H., David, J., 2009. Paleo- to Mesoarchean basement recycling and terrane definition in the Northeastern Superior Province, Québec, Canada. Precambrian Research 168, 23–44.

Bolhar, R., Kamber, B.S., Moorbath, S., Fedo, C.M., Whitehouse, M.J., 2004. Characterisation of early Archaean chemical sediments by trace element signatures. Earth and Planetary Science Letters 222, 43–60.

Bowring, S.A., Williams, I.S., 1999. Priscoan (4.00–4.03 Ga) orthogneisses from northwestern Canada. Contributions to Mineralogy and Petrology 134, 3–16.

Boyet, M., Carlson, R.W., 2006. A new geochemical model for the Earth's mantle inferred from ^{146}Sm–^{142}Nd systematics. Earth and Planetary Science Letters 250, 254–268.

Boyet, M., Blichert-Toft, J., Rosing, M., Storey, M., Télouk, P., Albarède, F., 2003. ^{142}Nd evidence for early Earth differentiation. Earth and Planetary Science Letters 214, 427–442.

Bridgewater, D., Schiötte, L., 1991. The Archean gneiss complex of northern Labrador: a review of current results, ideas and problems. Bulletin of the Geological Society of Denmark 39, 153–166.

Bruland, K.W., Lohan, M.C., 2004. The control of trace metals in seawater. In: Elderfield, H. (Ed.), The Oceans and Marine Geochemistry, The Treatise of Geochemistry, pp. 33–47.

Bucher, K., Frey, M., 2002. Petrogenesis of Metamorphic Rocks. Springer Verlag.

Bullen, T.D., White, A.F., Childs, C.W., Vivit, D.V., Schulz, M.S., 2001. Demonstration of significant abiotic iron isotope fractionation in nature. Geology 29, 699–702.

Cairns-Smith, A.G., 1978. Precambrian solution photochemistry, inverse segregation, and banded iron formations. Nature 276, 807–808.

Campbell, I.H., Griffiths, R.W., 1992. The changing nature of mantle hotspots through time: implications for the chemical evolution of the mantle. Journal of Geology 100, 497–523.

Canfield, D.E., 2005. An early history of atmospheric oxygen: homage to Robert M. Garrels. Annual Reviews in Earth and Planetary Science 33, 1–36.

Caro, G., Bourdon, B., Birck, J.-L., Moorbath, S., 2006. High-precision $^{142}Nd/^{144}Nd$ measurements in terrestrial rocks: constraints on the early differentiation of the Earth's mantle. Geochimica et Cosmochimica Acta 70, 164–191.

Cates, N.L., Mojzsis, S.J., 2006. Chemical and Isotopic Evidence for widespread Eoarchean metasedimentary enclaves in southern West Greenland. Geochimica et Cosmochimica Acta 70, 4229–4257.

Cates, N.L., Mojzsis, S.J., 2007. Pre-3750 Ma supracrustal rocks from the Nuvvuagittuq supracrustal belt, northern Québec. Earth and Planetary Science Letters 255, 9–21.

Cates, N.L., Mojzsis, S.J., 2009. Metamorphic zircon, trace elements and Neoarchean metamorphism in the ca. 3.75 Ga Nuvvuagittuq supracrustal belt, Québec (Canada). Chemical Geology 261, 99–114.

Cates, N.L., Mojzsis, S.J., Ziegler, K., Schmitt, A., in press. Origin of sediments from the Nuvvuagittuq Supracrustal Belt (Quebec, Canada) and maximum ages from detrital zircon. Earth and Planetary Science Letters.
Cloud, P., 1973. Paleoecological significance of the banded iron-formation. Economic Geology 68, 1135–1143.
Craddock, P.R., Dauphas, N., 2011. Iron and carbon isotope evidence for microbial iron respiration throughout the Archean. Earth and Planetary Science Letters 303, 121–132.
Croal, L.R., Johnson, C.M., Beard, B.L., Newman, D.K., 2004. Iron isotope fractionation by Fe(II)-oxidizing photoautotrophic bacteria. Geochimica et Cosmochimica Acta 68, 1227–1242.
Danielson, A., Möller, P., Dulski, P., 1992. The europium anomalies in banded iron formations and the thermal history of the oceanic crust. Chemical Geology 97, 89–100.
daSilva, J.J.R.F., Williams, R.J.P., 2001. The Biological Chemistry of the Elements: The Inorganic Chemistry of Life, 2nd ed. Oxford University Press, Oxford.
Dauphas, N., Kasting, J.F., 2011. Low pCO_2 in the pore water, not in the Archean air. Nature 474, E1.
Dauphas, N., Rouxel, O., 2006. Mass spectrometry and natural variations of iron isotopes. Mass Spectrometry Reviews 25, 515–550.
Dauphas, N., van Zuilen, M., Wadhwa, M., Davis, A.M., Marty, B., Janney, P.E., 2004. Clues from Fe isotope variations on the origin of early Archean BIFs from Greenland. Science 306, 2077–2080.
Dauphas, N., Cates, N.L., Mojzsis, S.J., Busigny, V., 2007a. Identification of chemical sedimentary protoliths using iron isotopes in the >3750 Ma Nuvvuagittuq supracrustal belt, Canada. Earth and Planetary Science Letters 254, 358–376.
Dauphas, N., van Zuilen, M., Busigny, V., Lepland, A., Wadhwa, M., Janney, P.E., 2007b. Iron isotope, major and trace element characterization of early Archean supracrustal rocks from SW Greenland: protolith identification and metamorphic overprint. Geochimica et Cosmochimica Acta 71, 4745–4770.
David, J., Parent, M., Stevenson, R., Nadeau, P., Godin, L., 2002. La séquence supracrustale de Porpoise Cove, région d'Inukjuak: un exemple unique de croûte paléo-archéenne (ca. 3.8 Ga) dans la Province du Supérieur. L'exploration Minérale au Québec, Notre Savoir, Vos Découvertes, Ministère des Ressources Naturelles, Québec, DV 2002-10.
David, J., Godin, L., Stevenson, R., O'Neil, J., Francis, D., 2009. U–Pb ages (3.8–2.7 Ga) and Nd isotope data from the newly identified Eoarchean Nuvvuagittuq supracrustal belt, Superior Craton, Canada. Geological Society of America Bulletin 121, 150–163.
Derry, L.A., Jacobsen, S.B., 1990. The chemical evolution of Precambrian seawater: evidence from REEs in banded iron formations. Geochimica et Cosmochimica Acta 54, 2965–2977.
Douville, E., Bienvenu, P., Charlou, J.L., Donval, J.P., Fouquet, Y., Appriou, P., Gamo, T., 1999. Yttrium and rare earth elements in fluids from various deep-sea hydrothermal systems. Geochimica et Cosmochimica Acta 63, 627–643.
Dupont, C.L., Butcher, A., Valas, R.E., Bourne, P.E., Caetano-Anollés, G., 2010. History of biological metal utilization inferred through phylogenomic analysis of protein structures. Proceedings of the National Academy of Sciences 107, 10567–10572.
Dyer, J.A., Trivedi, P., Scrivner, N.C., Sparks, D.L., 2004. Surface complexation modeling of zinc sorption onto ferrihydrite. Journal of Colloid and Interface Science 270, 56–65.
Dymek, R.F., Klein, C., 1988. Chemistry, petrology and origin of banded iron-formation lithologies from the 3800 MA isua supracrustal belt, West Greenland. Precambrian Research 39, 247–302.
Elliott, T., Plank, T., Zindler, A., White, W., Bourdon, B., 1997. Element transport from slab to volcanic front at the Mariana arc. Journal of Geophysical Research 102, 14991–15019.
Ewers, W.E., Morris, R.C., 1981. Studies of the Dales Gorge Member of the Brockman Iron Formation, Western Australia. Economic Geology 76, 1929–1953.
Fedo, C.M., Whitehouse, M.J., 2002. Metasomatic origin of quartz–pyroxene rock, Akilia, Greenland, and implications for Earth's earliest life. Science 296, 1448–1452.
Frei, R., Polat, A., 2007. Source heterogeneity for the major components of 3.7 Ga banded iron formations (Isua Greenstone Belt, Western Greenland): tracing the nature of interacting water masses in BIF formation. Earth and Planetary Science Letters 253, 266–281.
Govindaraju, K., 1994. Compilation of working values and sample description for 383 geostandard. Geostand. Newsl. 18, 1–158.
Guitreau, M., Blichert-Toft, J., Martin, H., Mojzsis, S., Albarede, F., 2012. Hafnium isotope evidence from Archean granitic rocks for deep-mantle origin of continental crust. Earth and Planetary Science Letters 337–338, 211–223.
Haase, C.S., 1982. Metamorphic petrology of the Negaunee Iron Formation, Marquette District, northern Michigan; mineralogy, metamorphic reactions, and phase equilibria. Economic Geology 77, 60–81.
Hahm, D., Hilton, D.R., Castillo, P.R., Hawkins, J.W., Hanan, B.B., Hauri, E.H., 2012. An overview of the volatile systematics of the Lau Basin — resolving the effects of source variation, magmatic degassing and crustal contamination. Geochimica et Cosmochimica Acta 85, 88–113.
Hamilton, P.J., O'Nions, R.K., Bridgwater, D., Nutman, A., 1983. Sm–Nd studies of Archaean metasediments and metavolcanics from West Greenland and their implications for the Earth's early history. Earth and Planetary Science Letters 62, 263–272.
Harley, S.L., Black, L.P., 1997. A revised Archean chronology for the Napier Complex, Enderby Land, from SHRIMP ion-microprobe studies. Antarctic Science 9, 74–91.
Heimann, A., Johnson, C.M., Beard, B.L., Valley, J.W., Roden, E.E., Spicuzza, M.J., Beukes, N.J., 2010. Fe, C, and O isotope compositions of banded iron formation carbonates demonstrate a major role for dissimilatory iron reduction in 2.5 Ga marine environments. Earth and Planetary Science Letters 294, 8–18.
Holland, H.D., 2002. Volcanic gases, black smokers, and the great oxidation event. Geochimica et Cosmochimica Acta 66, 3811–3826.
Holland, H.D., 2009. Why the atmosphere became oxygenated: a proposal. Geochimica et Cosmochimica Acta 73, 5241–5255.
Horita, J., 2005. Some perspectives on isotope biosignatures for early life. Chemical Geology 218, 171–186.
Hoskin, P.W.O., Schaltegger, U., 2003. The composition of zircon and igneous and metamorphic petrogenesis. Reviews in Mineralogy and Geochemistry 53, 27–62.
Iizuka, T., Komiya, T., Ueno, Y., Katayama, I., Uehara, Y., Maruyama, S., Hirata, T., Johnson, S.P., Dunkley, D.J., 2007. Geology and zircon geochronology of the Acasta Gneiss Complex, northwestern Canada: new constraints on its tectonothermal history. Precambrian Research 153, 179–208.
Isley, A.E., Abbott, D.H., 1999. Plume-related mafic volcanism and the deposition of banded iron formation. Journal of Geophysical Research 104, 15461–15477.
Jahn, B.M., Auvray, B., Cornichet, J., Bai, Y.L., Shen, Q.H., Liu, D.Y., 1987. 3.5 Ga old amphibolites from eastern Hebei Province, China: field occurrence, petrography, Sm–Nd isochron age and REE geochemistry. Precambrian Research 34, 311–346.
James, H.L., 1955. Zones of regional metamorphism in the Precambrian of Northern Michigan. Geological Society of America Bulletin 66, 1455–1488.
Johannesson, K.H., Hawkins Jr., D.L., Cortés, A., 2006. Do Archean chemical sediments record ancient seawater rare earth element patterns? Geochimica et Cosmochimica Acta 70, 871–890.
Johnson, C., Beard, B., Beukes, N., Klein, C., O'Leary, J., 2003. Ancient geochemical cycling in the Earth as inferred from Fe isotope studies of banded iron formations from the Transvaal Craton. Contributions to Mineralogy and Petrology 144, 523–547.
Johnson, C.M., Beard, B.L., Klein, C., Beukes, N.J., Roden, E.E., 2008. Iron isotopes constrain biologic and abiologic processes in banded iron formation genesis. Geochimica et Cosmochimica Acta 72, 151–169.
Kaiyi, W., Windley, B.F., Sills, J.D., Yuehua, Y., 1990. The Archaean gneiss complex in E. Hebei Province, North China: geochemistry and evolution. Precambrian Research 48, 245–265.
Kappler, A., Pasquero, C., Konhauser, K.O., Newman, D.K., 2005. Deposition of banded iron formations by anoxygenic phototrophic Fe(II)-oxidizing bacteria. Geology 33, 865–868.
Kerrich, R., Polat, A., 2006. Archean greenstone-tonalite duality: thermochemical mantle convection models or plate tectonics in the early Earth global dynamics? Tectonophysics 415, 141–165.
Kerrich, R., Said, N., Manikyamba, C., Wyman, D., in press. Sampling oxygenated Archean hydrosphere: implications from fractionations of Th/U and Ce/Ce^* in hydrothermally altered volcanic sequences. Gondwana Research.
Kinny, P.D., Williams, I.S., Froude, D.O., Ireland, T.R., Compston, W., 1988. Early Archaean zircon ages from orthogneisses and anorthosites at Mount Narryer, Western Australia. Precambrian Research 38, 325–341.
Kinoshita, N., Paul, M., Alcorta, M., Bowers, M., Collon, P., Deibel, C.M., DiGiovine, B., Goriely, S., Greene, J.P., Henderson, D.J., Jiang, C.L., Kashiv, Y., Kay, B.P., Lee, H.Y., Marley, S.T., Nakanishi, T., Pardo, R.C., Patel, N., Rehm, K.E., Robertson, D., Scott, R., Schmitt, C., Tang, X.D., Ugalde, C., Vondrasek, R., 2012. New AMS method to measure the atom ratio $^{146}Sm/^{147}Sm$ for a half-life determination of ^{146}Sm. Nuclear Instruments and Methods in Physics Research Section B: Beam Interactions with Materials and Atoms.
Kita, N.T., Huberty, J.M., Kozdon, R., Beard, B.L., Valley, J.W., 2011. High-precision SIMS oxygen, sulfur and iron stable isotope analyses of geological materials: accuracy, surface topography and crystal orientation. Surface and Interface Analysis 43, 427–431.
Klein, C., 1973. Changes in mineral assemblages with metamorphism of some banded Precambrian iron-formations. Economic Geology 68, 1075–1088.
Klein, C., 2005. Some Precambrian banded iron-formations (BIFs) from around the world: their age, geologic setting, mineralogy, metamorphism, geochemistry, and origins. American Mineralogist 90, 1473–1499.
Koehler, I., Papineau, D., Posth, N., Kappler, A., 2009. Lab simulations of long term diagenetic fate of biomass in banded iron formations. Goldschmidt Conference Abstracts A674.
Konhauser, K.O., Hamade, T., Raiswell, R., Morris, R.C., Ferris, F.G., Southam, G., Canfield, D.E., 2002. Could bacteria have formed the Precambrian banded iron formations? Geology 30, 1079–1082.
Konhauser, K.O., Amskold, L., Lalonde, S.V., Posth, N.R., Kappler, A., Anbar, A., 2007. Decoupling photochemical Fe(II) oxidation from shallow-water BIF deposition. Earth and Planetary Science Letters 258, 87–100.
Konhauser, K.O., Pecoits, E., Lalonde, S.V., Papineau, D., Nisbet, E.G., Barley, M.E., Arndt, N.T., Zahnle, K., Kamber, B.S., 2009. Oceanic nickel depletion and a methanogen famine before the Great Oxidation Event. Nature 458, 750–753.
Korenaga, J., 2011. Thermal evolution with a hydrating mantle and the initiation of plate tectonics in the early Earth. Journal of Geophysical Research 116, B12403.
Kump, L.R., Barley, M.E., 2007. Increased subaerial volcanism and the rise of atmospheric oxygen 2.5 billion years ago. Nature 448, 1033–1036.
Lackschewitz, K.S., Devey, C.W., Stoffers, P., Botz, R., Eisenhauer, A., Kummetz, M., Schmidt, M., Singer, A., 2004. Mineralogical, geochemical and isotopic characteristics of hydrothermal alteration processes in the active, submarine, felsic-hosted PACMANUS field, Manus Basin, Papua New Guinea. Geochimica et Cosmochimica Acta 68, 4405–4427.
Law, J., Phillips, N., 2006. Witwatersrand gold-pyrite-uraninite deposits do not support a reducing Archean atmosphere. In: Kesler, S.E., Ohmoto, H. (Eds.), Evolution of Early Earth's Atmosphere, Hydropshere, and Biosphere — Constraints from Ore Deposits.Geological Society of America Memoir 121–141.

Le Roux, V., Lee, C.T.A., Turner, S.J., 2010. Zn/Fe systematics in mafic and ultramafic systems: implications for detecting major element heterogeneities in the Earth's mantle. Geochimica et Cosmochimica Acta 74, 2779–2796.
Lepland, A., Van Zuilen, M.A., Philippot, P., 2011. Fluid-deposited graphite and its geobiological implications in early Archean gneiss from Akilia, Greenland. Geobiology 9, 2–9.
Liu, D.Y., Nutman, A.P., Compston, W., Wu, J.S., Shen, Q.H., 1992. Remnants of ≥3800 Ma crust in the Chinese part of the Sino-Korean craton. Geology 20, 339–342.
Liu, D.Y., Wan, Y.S., Wu, J.S., Wilde, S.A., Zhou, H.Y., Dong, C.Y., Yin, X.Y., 2007. Chapter 3.5 Eoarchean rocks and zircons in the North China Craton. In: Martin, J., van Kranendonk, R.H.S., Vickie, C.B. (Eds.), Developments in Precambrian Geology. Elsevier, pp. 251–273.
Lowe, D.R., Byerly, G.R., 1999. Stratigraphy of the West-central Part of the Barberton Greenstone Belt. Geological Society of America, South Africa.
MacRae, N.D., Nesbitt, H.W., Kronberg, B.I., 1992. Development of a positive Eu anomaly during diagenesis. Earth and Planetary Science Letters 109, 585–591.
Manning, C.E., Mojzsis, S.J., Harrison, T.M., 2006. Geology, age and origin of supracrustal rocks at Akilia, West Greenland. American Journal of Science 306, 303–366.
McKeegan, K.D., Kudryavtsev, A.B., Schopf, J.W., 2007. Raman and ion microscopic imagery of graphitic inclusions in apatite from older than 3830 Ma Akilia supracrustal rocks, west Greenland. Geology 35, 591–594.
McKenzie, D., Weiss, N., 1975. Speculations on the thermal and tectonic history of the earth. Geophysical Journal of the Royal Astronomical Society 42, 131–174.
Mloszewska, A.M., Pecoits, E., Cates, N.L., Mojzsis, S.J., O'Neil, J., Robbins, L.J., Konhauser, K.O., 2012. The composition of Earth's oldest iron formations: the Nuvvuagittuq Supracrustal Belt (Québec, Canada). Earth and Planetary Science Letters 317–318, 331–342.
Mojzsis, S.J., Arrhenius, G., McKeegan, K.D., Harrison, T.M., Nutman, A.P., Friend, C.R.L., 1996. Evidence for life on Earth before 3,800 million years ago. Nature 384, 55–59.
Moorbath, S., Allaart, J.H., Bridgwater, D., McGregor, V.R., 1977. Rb–Sr ages of early Archaean supracrustal rocks and Amitsoq gneisses at Isua. Nature 270, 43–45.
Myers, J.S., Williams, I.R., 1985. Early Precambrian crustal evolution at Mount Narryer, Western Australia. Precambrian Research 27, 153–163.
Nisbet, E.G., Fowler, C.M.R., 1996. The hydrothermal imprint on life: did heat-shock proteins, metalloproteins and photosynthesis begin around hydrothermal vents? Geological Society, London, Special Publications 118, 239–251.
Nutman, A.P., Fryer, B.J., Bridgewater, D., 1989. The early Archean Nulliak (supracrustal) Assemblage, northern Labrador. Canadian Journal of Earth Sciences 26.
Nutman, A.P., McGregor, V.R., Friend, C.R.L., Bennett, V.C., Kinny, P.D., 1996. The Itsaq Gneiss Complex of southern West Greenland; the world's most extensive record of early crustal evolution (3900–3600 Ma). Precambrian Research 78, 1–39.
Nutman, A.P., Bennett, V.C., Friend, C.R.L., Rosing, M.T., 1997. 3710 and ≥3790 Ma volcanic sequences in the Isua (Greenland) supracrustal belt; structural and Nd isotope implications. Chemical Geology. 3–4, 271–287.
Nutman, A.P., Bennett, V.C., Friend, C.R.L., McGregor, V.R., 2000. The early Archaean Itsaq Gneiss Complex of southern West Greenland: the importance of field observations in interpreting age and isotopic constraints for early terrestrial evolution. Geochimica et Cosmochimica Acta 64, 3035–3060.
Nutman, A.P., Friend, C.R.L., Barker, S.L.L., McGregor, V.R., 2004. Inventory and assessment of Palaeoarchaean gneiss terrains and detrital zircons in southern West Greenland. Precambrian Research 135, 281–314.
Ohmoto, H., Watanabe, Y., Yamaguchi, K.E., Naraoka, H., Haruna, M., Kakewaga, T., Hayashi, K.-i, Kato, Y., 2006. Chemical and biological evolution of early Earth: constraints from banded iron formations. In: Kesler, S.E., Ohmoto, H. (Eds.), Evolution of Earth's Atmosphere, Hydrosphere, and Biosphere—Constraints from Ore Deposits.Geological Society of America Memoir 291–337.
O'Neil, J., personal communication.
O'Neil, J., Maurice, C., Stevenson, R.K., Larocque, J., Cloquet, C., David, J., Francis, D., 2007. The Geology of the 3.8 Ga Nuvvuagittuq (Porpoise Cove) Greenstone Belt, Northeastern Superior Province, Canada. Developments in Precambrian Geology 15, 219–250.
O'Neil, J., Carlson, R.W., Francis, D., Stevenson, R.K., 2008. Neodymium-142 evidence for Hadean mafic crust. Science 321, 1828–1831.
O'Neil, J., Francis, D., Carlson, R., 2011. Implications of the Nuvvuagittuq Greenstone Belt for the formation of Earth's early crust. Journal of Petrology 52, 985–1009.
Papineau, D., 2010. Mineral environments on the earliest Earth. Elements 6, 25–30.
Papineau, D., De Gregorio, B.T., Cody, G.D., Fries, M.D., Mojzsis, S.J., Steele, A., Stroud, R.M., Fogel, M.L., 2010a. Ancient graphite in the Eoarchean quartz–pyroxene rocks from Akilia in southern West Greenland I: petrographic and spectroscopic characterization. Geochimica et Cosmochimica Acta 74, 5862–5883.
Papineau, D., De Gregorio, B.T., Stroud, R.M., Steele, A., Pecoits, E., Konhauser, K., Wang, J., Fogel, M.L., 2010b. Ancient graphite in the Eoarchean quartz–pyroxene rocks from Akilia in southern West Greenland II: isotopic and chemical compositions and comparison with Paleoproterozoic banded iron formations. Geochimica et Cosmochimica Acta 74, 5884–5905.
Papineau, D., De Gregorio, B.T., Cody, G.D., O'Neil, J., Steele, A., Stroud, R.M., Fogel, M.L., 2011. Young poorly crystalline graphite in the >3.8-Gyr-old Nuvvuagittuq banded iron formation. Nature Geoscience 4, 376–379.
Percival, J.A., Skulski, T., 2000. Tectonothermal evolution of the Northern Minto block, Superior Province, Quebec, Canada. The Canadian Mineralogist 38, 345–378.
Percival, J.A., Stern, R.A., Skulski, T., Card, K.D., Mortensen, J.K., Begin, N.J., 1994. Minto block, Superior province: missing link in deciphering assembly of the craton at 2.7 Ga. Geology 22, 839–842.
Perry, E.C., Ahmad, S.N., 1977. Carbon isotope composition of graphite and carbonate minerals from 3.8-AE metamorphosed sediments, Isukasia, Greenland. Earth and Planetary Science Letters 36, 280–284.
Petford, N., 1996. Dykes or diapirs? Earth and Environmental Science Transactions of the Royal Society of Edinburgh 87, 105–114.
Planavsky, N., Bekker, A., Rouxel, O.J., Kamber, B., Hofmann, A., Knudsen, A., Lyons, T.W., 2010a. Rare earth element and yttrium compositions of Archean and Paleoproterozoic Fe formations revisited: new perspectives on the significance and mechanisms of deposition. Geochimica et Cosmochimica Acta 74, 6387–6405.
Planavsky, N.J., Rouxel, O.J., Bekker, A., Lalonde, S.V., Konhauser, K.O., Reinhard, C.T., Lyons, T.W., 2010b. The evolution of the marine phosphate reservoir. Nature 467, 1088–1090.
Planavsky, N.J., McGoldrick, P., Scott, C.T., Li, C., Reinhard, C.T., Kelly, A.E., Chu, X., Bekker, A., Love, G.D., Lyons, T.W., 2011. Widespread iron-rich conditions in the mid-Proterozoic ocean. Nature 477, 448–451.
Polat, A., Frei, R., 2005. The origin of early Archean banded iron formations and of continental crust, Isua, southern West Greenland. Precambrian Research 138, 151–175.
Ragsdale, S.W., Kumar, M., 1996. Nickel-containing carbon monoxide dehydrogenase/acetyl-CoA synthase. Chemical Reviews 96, 2515–2539.
Rosing, M.T., 1999. ^{13}C-depleted carbon microparticles in >3700-Ma Sea-floor sedimentary rocks from West Greenland. Science 283, 674–676.
Rosing, M.T., Bird, D.K., Sleep, N.H., Bjerrum, C.J., 2010. No climate paradox under the faint early Sun. Nature 464, 744–747.
Ross, M., Papike, J.J., Shaw, K.W., 1969. Exsolution textures in amphiboles as indicators of subsolidus thermal histories. Mineralogical Society of America Special Paper 2, 275–299.
Roth, A.S.G., Bourdon, B., Mojzsis, S.J., Touboul, M., Sprung, P., Guitreau, M., Blichert-Toft, J., in press. Inherited 142Nd anomalies in Eoarchean protoliths. Earth and Planetary Science Letters.
Saito, M.A., Sigman, D.M., Morel, F.M.M., 2003. The bioinorganic chemistry of the ancient ocean: the co-evolution of cyanobacterial metal requirements and biogeochemical cycles at the Archean–Proterozoic boundary? Inorganica Chimica Acta 356, 308–318.
Schidlowski, M., 1988. A 3,800-million-year isotopic record of life from carbon in sedimentary rocks. Nature 333, 313–318.
Schidlowski, M., Appel, P.W.U., Eichmann, R., Junge, C.E., 1979. Carbon isotope geochemistry of the 3.7×10^9-yr-old Isua sediments, West Greenland: implications for the Archaean carbon and oxygen cycles. Geochimica et Cosmochimica Acta 43, 189–199.
Schiotte, L., Compston, D., Bridgewater, D., 1989. Ion U–Th–Pb zircon dating of polymetamorphic orthogneisses from northern Labrador, Canada. Canadian Journal of Earth Sciences 26, 1533–1556.
Scott, C.T., Planavsky, N.J., Dupont, C.L., Kendall, B., Gill, B., Robbins, L.J., Bekker, A., Konhauser, K.O., Poulton, S.W., Wing, B., Anbar, A., Lyons, T.W., in press. Marine zinc bioavailability through time. Nature Geoscience.
Simard, M., Parent, M., David, J., Sharma, K.N.M., 2003. Géologie de la région de la rivière Innuksuac (34K et 34L). Ministère des Ressources naturelles, Québec RG 2002-10, p. 46.
Steinhoefel, G., von Blanckenburg, F., Horn, I., Konhauser, K.O., Beukes, N.J., Gutzmer, J., 2010. Deciphering formation processes of banded iron formations from the Transvaal and the Hamersley successions by combined Si and Fe isotope analysis using UV femtosecond laser ablation. Geochimica et Cosmochimica Acta 74, 2677–2696.
Stevenson, R.K., David, J., Parent, M., 2006. Crustal evolution of the western Minto Block, northern Superior Province, Canada. Precambrian Research 145, 229–242.
Trendall, A.F., 2009. The significance of iron-formation in the Precambrian stratigraphic record. Precambrian Sedimentary Environments. Blackwell Publishing Ltd, pp. 33–66.
Trivedi, P., Axe, L., 2001. Ni and Zn Sorption to amorphous versus crystalline iron oxides: macroscopic studies. Journal of Colloid and Interface Science 244, 221–229.
Valley, J.W., 1986a. Stable isotope geochemistry of metamorphic rocks. Reviews in Mineralogy 16, 445–489.
Valley, J.W., 1986b. Stable isotope geochemistry of metamorphic rocks. Reviews in Mineralogy and Geochemistry 16, 445–489.
van Zuilen, M.A., Lepland, A., Arrhenius, G., 2002. Reassessing the evidence for the earliest traces of life. Nature 418, 627–630.
van Zuilen, M.A., Lepland, A., Teranes, J., Finarelli, J., Wahlen, M., Arrhenius, G., 2003. Graphite and carbonates in the 3.8 Ga old Isua Supracrustal Belt, southern West Greenland. Precambrian Research 126, 331–348.
van Zuilen, M.A., Mathew, K., Wopenka, B., Lepland, A., Marti, K., Arrhenius, G., 2005. Nitrogen and argon isotopic signatures in graphite from the 3.8-Ga-old Isua Supracrustal Belt, Southern West Greenland. Geochimica et Cosmochimica Acta 69, 1241–1252.
Welch, S.A., Beard, B.L., Johnson, C.M., Braterman, P.S., 2003. Kinetic and equilibrium Fe isotope fractionation between aqueous Fe(II) and Fe(III). Geochimica et Cosmochimica Acta 67, 4231–4250.
Whitehouse, M.J., Fedo, C.M., 2007. Microscale heterogeneity of Fe isotopes in >3.71 Ga banded iron formation from the Isua Greenstone Belt, southwest Greenland. Geology 35, 719–722.
Widdel, F., Schnell, S., Heising, S., Ehrenreich, A., Assmus, B., Schink, B., 1993. Ferrous iron oxidation by anoxygenic phototrophic bacteria. Nature 362, 834–836.
Wilde, S.A., Valley, J.W., Peck, W.H., Grahams, C.M., 2001. Evidence from detrital zircons for the existence of continental crust and oceans on the Earth 4.4 Gyr ago. Nature 409, 175–178.
Xu, Y., Axe, L., Boonfueng, T., Tyson, T.A., Trivedi, P., Pandya, K., 2007. Ni(II) complexation to amorphous hydrous ferric oxide: an X-ray absorption spectroscopy study. Journal of Colloid and Interface Science 314, 10–17.

Yamashita, K., Creaser, R.A., Villeneuve, M.E., 2000. Integrated Nd isotopic and U–Pb detrital zircon systematics of clastic sedimentary rocks from the Slave Province, Canada: evidence for extensive crustal reworking in the early- to mid-Archean. Earth and Planetary Science Letters 174, 283–299.
Zahnle, K.J., 2006. Earth's earliest atmosphere. Elements 2, 217–222.
Zhai, M., Windley, B.F., 1990. The Archaean and early Proterozoic banded iron formations of North China: their characteristics, geotectonic relations, chemistry and implications for crustal growth. Precambrian Research 48, 267–286.

Aleksandra Mloszewska is a PhD student at the University of Alberta (Edmonton, Alberta) under the supervision of Dr. Kurt Konhauser. She completed her undergraduate degree at Queen's University (Kingston, Ontario) in geology and biology, and received her MSc at McGill University (Montreal, Québec), studying early shell degradation in temperate marine environments under Dr. Mairi Best. Her doctoral work includes the study of Eoarchean seawater composition and its influence on early metalloenzyme evolution. Her research focuses on using banded iron formation geochemistry to derive ancient seawater composition, and integrating this information with thermodynamic as well as molecular and biological models to a more dynamic and accurate picture of early seawater composition and its influences on the evolution of life. Her research is supported by a post-graduate scholarship from the National Science and Engineering Research Council of Canada.

Stephen James Mojzsis is a professor of geochemistry in the Department of Geological Sciences at the University of Colorado (Boulder), and currently on academic leave at the Laboratoire de Géologie de Lyon (École Normale Supérieur de Lyon & Université Claude Bernard Lyon 1). He received his PhD at the Scripps Institute of Oceanography (UC San Diego) in 1997. He subsequently became a postdoctoral fellow in the Department of Earth and Space Sciences at the University of California (Los Angeles), and in 2000, joined the faculty at the Department of Geological Sciences at the University of Colorado at Boulder. His research includes: the application of stable/radiogenic isotope and trace element geochemistry in mineral chemistry and metamorphic petrology for the documentation of ancient protoliths and studying atmosphere–ocean–crust interactions over geologic time; geochronology related to crustal evolution and petrogenesis via U–Th–Pb zircon and other isotopic techniques; documentation of field relationships of complex granite gneiss terranes by high-resolution mapping (1:5–1:1000) to guide sampling; MC-ICP-MS for coupled Hf and Nd; cosmochemistry viz. mineralogy of lunar, Martian and asteroidal meteorites; models for thermal structure of planetary objects from the Earth, to the Moon, asteroids, Kuiper Belt/Trans-Neptunian Objects; pre- and post-closure temperature thermal chemical diffusion modeling of minerals; evolution of atmospheric oxygen as it relates to the origin and early evolution of biogeochemical cycles; and conditions for the origin of life on Earth and Earth-like planets, moons and icy objects.

Ernesto Pecoits is Agouron geobiology post-doctoral fellow in the Department of Earth and Atmospheric Sciences at the University of Alberta. As a Precambrian geologist with expertise in stratigraphy, geomicrobiology and geochemistry, he is broadly interested in Precambrian life and environments and the relationship between the two. By integrating geological observations and tracking biological and chemical signals preserved in sedimentary rocks the ultimate goal of his research is to unravel the paleoenvironmental conditions prevailing in the Earth's deep past and surrounding the evolution of early life and animals.

Dominic Papineau is an Assistant Professor in the Department of Earth and Environmental Sciences at Boston College, and a Visiting Scientist at the Carnegie Institution of Washington. He received his PhD from the University of Colorado (Boulder) in 2006, and subsequently became a Research Associate at the Carnegie Institution of Washington until 2011, when he joined the faculty at Boston College. The overarching goals of his research are: 1) to unravel the details of the co-evolution of microbial life and multicellular organisms on the early Earth with changing atmospheric/oceanic oxidation states, climate upheavals, large igneous province occurrences, and other global biogeochemical perturbations, and 2) to search for a record of extra-terrestrial microbial life on early Mars. Dr. Papineau has field experience in remote Precambrian terrains from around the world including Greenland, Rajasthan (India), South Africa, northern Finland, Western Australia, northern Québec (Canada) and Antarctica. He performs in situ micro-analyses on polished thin sections, rock slabs and micro-drilled powders with a variety of state-of-the-art instruments including mass spectrometers (IRMS, TIMS and ICPMS), electron beam instruments (EPMA, SEM and TEM), ion beam techniques (nanoSIMS, ims1270 and FIB) and spectroscopy (Raman, FTIR and STXM).

Nicolas Dauphas (http://originslab.org) is Professor at the University of Chicago in the Department of the Geophysical Sciences and the Enrico Fermi Institute. After attending École Nationale Supérieure de Géologie (Nancy, France), he received a PhD in geochemistry in 2002 from the Centre de Recherches Pétrographiques et Géochimiques. A member of the University of Chicago faculty since 2004, he was the first to discover planetary scale nucleosynthetic anomalies for a refractory element and to recognize Mars as a planetary embryo. His research interests include cosmochemistry, geochronology, and non-traditional stable isotope geochemistry. His recent work has centered on the use of NRIXS spectroscopy to understand redox and structural controls on the iron isotopic compositions of magmas. He received numerous awards, including a Packard fellowship, the Nier prize, the Houtermans and Macelwane medals. He has authored some 70 scientific publications.

Kurt Konhauser is a Professor of Geomicrobiology in the Department of Earth and Atmospheric Sciences at the University of Alberta, Canada. He is Editor-in-Chief for the journal *Geobiology*, and author of the textbook *Introduction to Geomicrobiology* published by Wiley-Blackwell in 2007. His research focuses on the role of bacteria in modern mineral precipitation and elemental cycling, and how those same processes may have contributed to the preservation of early life forms and the formation of Precambrian banded iron formations. Other current interests include using Precambrian sediments as proxies for ancient seawater composition and evolution of the marine biosphere.